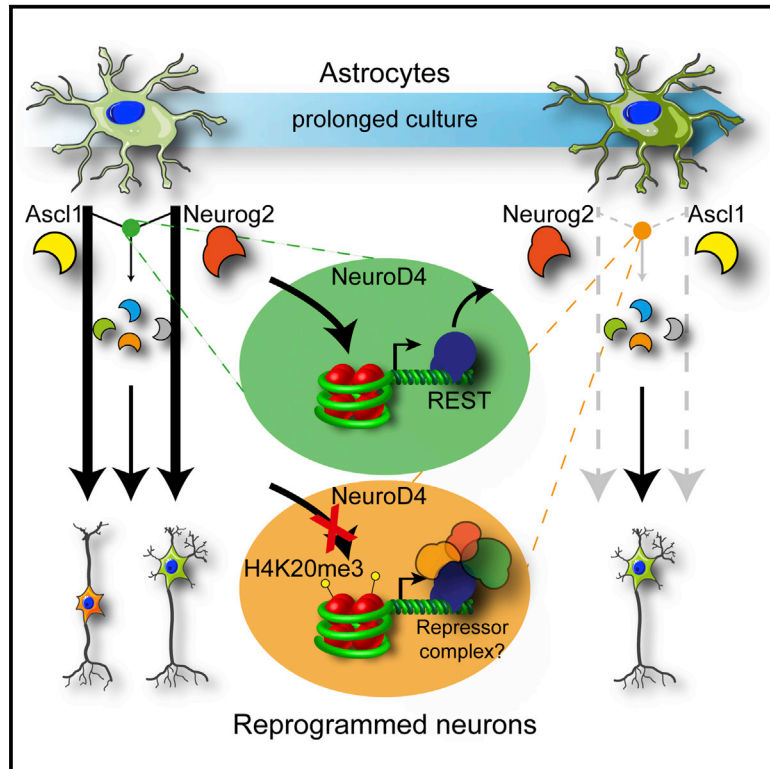


# Transcriptional Mechanisms of Proneural Factors and REST in Regulating Neuronal Reprogramming of Astrocytes

## Graphical Abstract



## Authors

Giacomo Masserdotti,  
Sébastien Gillotin, Bernd Sutor, ...,  
Benedikt Berninger,  
François Guillemot, Magdalena Götz

## Correspondence

francois.guillemot@crick.ac.uk (F.G.),  
magdalena.goetz@helmholtz-muenchen.de (M.G.)

## In Brief

Masserdotti et al. analyzed early transcriptional changes mediated by Neurog2 and Ascl1 during direct reprogramming of murine postnatal astrocytes into distinct neuronal subtypes in vitro. This led to the identification of shared downstream targets, including NeuroD4, capable of neuronal reprogramming of fibroblasts and human astrocytes, as well as mechanistic insight into how the repressor REST functions as a barrier in direct neuronal reprogramming.

## Accession Numbers

GSE60389

## Highlights

- Neurog2 and Ascl1 regulate largely non-overlapping neurogenic targets
- A subset of genes is required and sufficient to convert astrocytes and fibroblasts
- Neurog2 and REST compete for binding to the *NeuroD4* promoter
- REST deletion enhances Neurog2-mediated reprogramming in vitro



# Transcriptional Mechanisms of Proneural Factors and REST in Regulating Neuronal Reprogramming of Astrocytes

Giacomo Masserdotti,<sup>1,2,13</sup> Sébastien Gillotin,<sup>3,4,13</sup> Bernd Sutor,<sup>1</sup> Daniela Drechsel,<sup>3</sup> Martin Irmeler,<sup>5</sup> Helle F. Jørgensen,<sup>6</sup> Steffen Sass,<sup>7</sup> Fabian J. Theis,<sup>7,8</sup> Johannes Beckers,<sup>5,11</sup> Benedikt Berninger,<sup>9,10</sup> François Guillemot,<sup>3,14,\*</sup> and Magdalena Götz<sup>1,2,12,14,\*</sup>

<sup>1</sup>Physiological Genomics, Biomedical Center, University of Munich, 80336 Munich, Germany

<sup>2</sup>Institute for Stem Cell Research, Helmholtz Centre Munich, 85764 Neuherberg, Germany

<sup>3</sup>The Francis Crick Institute, Mill Hill Laboratory, The Ridgeway, London, NW7 1AA, UK

<sup>4</sup>Hutchison/MRC Research Center, University of Cambridge, Cambridge Biomedical Campus, Cambridge, CB2 0XZ, UK

<sup>5</sup>Institute of Experimental Genetics, Helmholtz Centre Munich, 85764 Neuherberg, Germany

<sup>6</sup>Department of Medicine, University of Cambridge, Cambridge, CB2 0QQ, UK

<sup>7</sup>Institute of Computational Biology, Helmholtz Centre Munich, 85764 Neuherberg, Germany

<sup>8</sup>Department of Mathematics, Technical University Munich, 85748 Garching, Germany

<sup>9</sup>Institute of Physiological Chemistry, University Medical Center of the Johannes Gutenberg University, D-55128 Mainz, Germany

<sup>10</sup>Focus Program Translational Neuroscience, Johannes Gutenberg University, D-55128 Mainz, Germany

<sup>11</sup>Center of Life and Food Sciences Weihenstephan, Technical University, 85354 Freising, Germany

<sup>12</sup>Munich Cluster for Systems Neurology "SyNergy," Ludwig Maximilian University of Munich, 80539 Munich, Germany

<sup>13</sup>Co-first author

<sup>14</sup>Co-senior author

\*Correspondence: [francois.guillemot@crick.ac.uk](mailto:francois.guillemot@crick.ac.uk) (F.G.), [magdalena.goetz@helmholtz-muenchen.de](mailto:magdalena.goetz@helmholtz-muenchen.de) (M.G.)

<http://dx.doi.org/10.1016/j.stem.2015.05.014>

This is an open access article under the CC BY license (<http://creativecommons.org/licenses/by/4.0/>).

## SUMMARY

Direct lineage reprogramming induces dramatic shifts in cellular identity, employing poorly understood mechanisms. Recently, we demonstrated that expression of Neurog2 or Ascl1 in postnatal mouse astrocytes generates glutamatergic or GABAergic neurons. Here, we take advantage of this model to study dynamics of neuronal cell fate acquisition at the transcriptional level. We found that Neurog2 and Ascl1 rapidly elicited distinct neurogenic programs with only a small subset of shared target genes. Within this subset, only NeuroD4 could by itself induce neuronal reprogramming in both mouse and human astrocytes, while co-expression with Insm1 was required for glutamatergic maturation. Cultured astrocytes gradually became refractory to reprogramming, in part by the repressor REST preventing Neurog2 from binding to the NeuroD4 promoter. Notably, in astrocytes refractory to Neurog2 activation, the underlying neurogenic program remained amenable to reprogramming by exogenous NeuroD4. Our findings support a model of temporal hierarchy for cell fate change during neuronal reprogramming.

## INTRODUCTION

During development, neuronal subtypes are generated typically in distinct regions with patterning cues initiating regional pro-

grams of neurogenesis (Martynoga et al., 2012). In the telencephalon, for example, stem and progenitor cells in the ventral region are instructed to express the transcription factors Ascl1, Gsx1/2, and Dlx1/2, which then regulate the specification of GABAergic projection and interneurons (for review see Imayoshi and Kageyama, 2014); in the dorsal telencephalon, progenitors express different transcription factors, such as Emx1/2, Pax6, and Neurog1/2, which regulate the specification of glutamatergic projection neurons (Schuurmans and Guillemot, 2002). Analysis of the transcriptional programs in mouse mutants revealed rather distinct transcriptional targets regulated by these transcription factors in the dorsal and ventral telencephalon (Gohlke et al., 2008). Whether this limited overlap is due to early divergence of these regions initiated by patterning signals, resulting in distinct transcriptional contexts, remains an open question. Neurons may be specified in a hierarchical manner, with the induction of common neuronal traits first, followed later by neuronal subtype features via a final set of transcription factors, such as terminal selector genes (Hobert, 2011). Conversely, distinct transcriptional regulators may specify different neuronal subtypes already at the onset of neuronal commitment, with relatively little overlap between transcriptional programs.

Direct reprogramming is especially well suited to examine the programs elicited by distinct transcription factors within the same cellular and epigenetic context. When expressed in astrocytes obtained from postnatal murine cerebral cortex gray matter, Ascl1 instructs GABAergic neurons, while Neurog2 elicits glutamatergic neurons (Berninger et al., 2007; Heinrich et al., 2010), thus making possible the identification of target genes involved in neuronal subtype specification within the same transcriptional background. In different cell types, such as fibroblasts, Ascl1 induces a glutamatergic neuronal fate in combination with Myt1L

and Brn2 in fibroblasts (Vierbuchen et al., 2010), while Neurog2 forces motor neuron generation in combination with forskolin and dorsomorphin (Liu et al., 2013). Thus, the cell of origin, with its specific epigenetic landscape, can play a role in defining the spectrum of reprogramming possibilities.

To date, the transcriptional programs elicited by direct lineage conversion toward neuronal fates are still largely elusive. Emerging evidences suggest an important role for epigenetic mechanisms as a hurdle to reprogramming (Wapinski et al., 2013; Xue et al., 2013). Large repressive protein complexes have been implicated in cell fate specification and differentiation: for instance, the REST/CoREST complex, known for its role in maintaining neural stem cells (Laugesen and Helin, 2014) and neuronal differentiation (Lu et al., 2014) has been shown to be the target of miRNA-mediated reprogramming of fibroblast into neurons (Xue et al., 2013). However, is it known neither when and how REST contributes to repress direct reprogramming, nor the mechanisms relevant in establishing reprogramming borders during cell differentiation.

To tackle these important questions, we examined the temporal regulation of genes at early stages of in vitro direct reprogramming of young postnatal astrocytes into neurons using tamoxifen-inducible forms of Ascl1 and Neurog2, which allowed the unraveling of the dynamics of transcriptional regulation as well as an understanding of the mechanisms involved in the failure to activate key targets in unresponsive astrocytes.

## RESULTS

### Activation of Neurog2ERT2 and Ascl1ERT2 Instructs Neurons from Glia

In order to investigate the early events of direct reprogramming, the cDNA of *Neurog2* and *Ascl1* was fused to the modified estrogen receptor ligand binding domain ERT2 (Raposo et al., 2015) and sub-cloned into a retroviral construct, together with the red fluorescent protein (DsRed-Expressed2, hereafter indicated as DsRed) (Berninger et al., 2007; Heinrich et al., 2010; Heins et al., 2002). Proliferating astrocytes were obtained from postnatal day (P)6–7 mouse cerebral cortex Gray Matter (GM), avoiding the White Matter (WM) and ventricular regions comprising endogenous neural stem cells (Imura et al., 2006). The purity of these cultures was previously assessed with various astrocytic markers and genetic fate mapping (Berninger et al., 2007; Heinrich et al., 2010; Heins et al., 2002) (see also Figures S1I and S1J). Moreover, cells infected with control retroviral vectors expressing GFP or DsRed showed a low proportion of Lewis X+ progenitors (3.9% ± 1.6% at day 2, Figures S1A–S1H) and did not generate any  $\beta$ III-tubulin+ neurons (0%, 250 cells counted/experiment, n = 8). Likewise, Neurog2ERT2-transduced or Ascl1ERT2-transduced cells remained GFAP+ and generated virtually no neurons after 1 week without 4-hydroxy-tamoxifen (OHT) addition (Figures 1B and 1E; quantification in Figures 1D and 1G, 0% with Neurog2ERT2 and 0.8% with Ascl1ERT2; Figures 1D and 1G). Thus, these cultures contain largely non-neurogenic proliferating astrocytes.

Treatment with OHT for 4 consecutive days elicited the highest efficiency of neuronal conversion, as assessed by morphology and  $\beta$ III-tubulin immunostaining (Figures 1C and 1F; quantification in Figures 1D and 1G; for shorter periods see Figures

S1K–S1M). Importantly, this OHT treatment of Neurog2ERT2- and Ascl1ERT2-transduced astroglia triggered similar reprogramming efficiency (40% of DsRed+ cells), thus providing a suitable system for the investigation of the transcriptional changes during reprogramming triggered by the two factors.

### Ascl1 and Neurog2 Induce Rapid but Distinct Transcriptional Programs in Astrocytes In Vitro

First, we analyzed the transcriptome of Neurog2ERT2- and Ascl1ERT2-transduced astroglial cultures after OHT-treatment for 4, 24, and 48 hr (Figure 1H; Figures S1N and S1O' for transduction efficiency). Activation of Neurog2ERT2 for 4 hr changed the expression of 199 probesets (fold change > 1.2, rawp (p value of the t-test statistics) < 0.01, Table S1), suggesting that transcriptional changes take place rapidly. This set of regulated genes was significantly enriched for the gene ontology (GO) terms (Huang et al., 2009) (as codified according to DAVID; <http://david.abcc.ncifcrf.gov>) associated with “regulation of cell proliferation,” “cell adhesion,” and, despite the early stage, “voltage-gated channel activity,” including genes expressed by excitable cells, such as *Scn8a* and *Cacna1d* (Table S2). At 24 hr, the number of Neurog2ERT2-regulated probesets increased further by 27% (253, fold change > 1.2, rawp < 0.01, Figure S1P, Table S1). At 48 hr a different group of probesets was regulated (Figure S1P, Table S1), such that only 6% of the 712 probesets regulated during the period analyzed showed an altered expression at two or more time points (43 probesets, Figure S1P). Thus, large-scale and dynamic changes in gene expression take place throughout the first 48 hr of direct neuronal reprogramming.

We then examined the transcriptome changes upon Ascl1ERT2 activation, which resulted in a higher number of regulated genes, possibly due to Ascl1 acting as a master and pioneering transcription factor (Wapinski et al., 2013). Rapid changes in gene expression were observed already at 4 hr (621 probesets, GO terms in Table S4), increased at 24 hr (1,148 probesets), and decreased at 48 hr (591 probesets; fold change > 1.2, rawp < 0.01, Figure S1P', Table S3). Overall, 13.5% of all the probesets altered at any time point after Ascl1ERT2 activation were significantly regulated at two time points at least (319 out of 2,360 probesets, Figure S1P', Table S3). Thus, Ascl1ERT2 also induced fast and dynamic changes in gene expression, suggesting a rapid change in cellular identity.

Of the probesets regulated by Neurog2ERT2 or Ascl1ERT2, only 1.34% was common to both factors at 4 hr after induction (Figure S1Q), 3.5% at 24 hr (Figures 1I and 1J), and 3.1% at 48 hr (Figure S1R). Overall, the probesets regulated by both transcription factors account for only 2.8% of all the probesets regulated at any time by either factor, demonstrating that the small overlap is not due to different kinetics of the Neurog2- and Ascl1-induced programs, but rather to the activation of largely different gene cascades.

GO terms associated with the small subset of targets common at 24 hr (49 probesets) were enriched for the terms “neuronal development” and “neurogenesis” (Figure S1S, Table S5) with 79% of them expressed in neurons and progenitors throughout the brain and 61% with a pan-neuronal expression (such as *Atoh8*, *Hes6*, *Insm1*, *NeuroD4*, *Prox1*, *Sox11*, and *Trnp1*; see Table S6). Selected candidates downstream of Neurog2ERT2 and

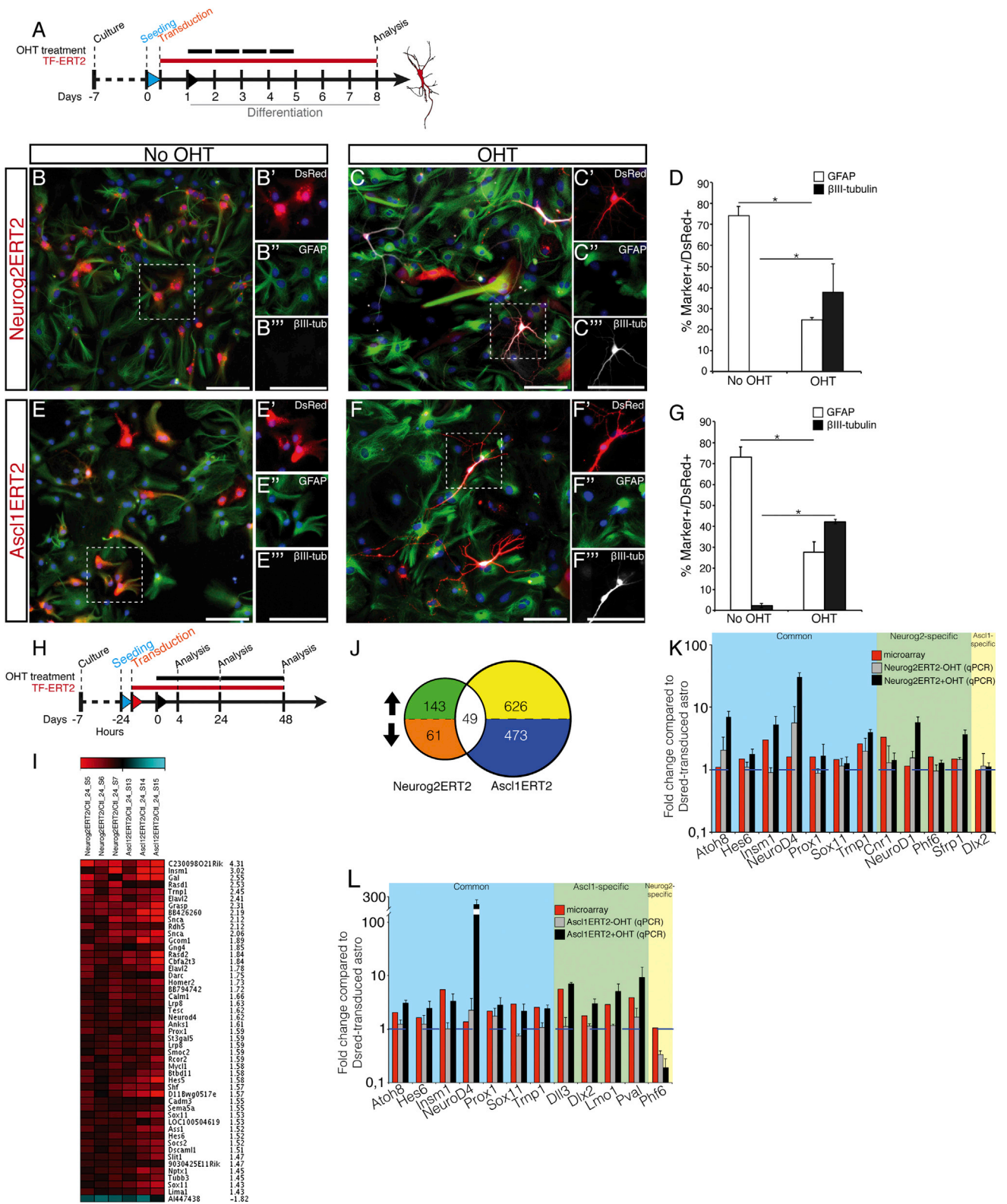


**Figure 1. Temporal Analysis of Genome-wide Transcription Changes in Astrocyte Reprogramming**

(A) Schematic representation of the experimental procedure inducing the activation of Neurog2ERT2-IRES-DsRed or Ascl1ERT2-IRES-DsRed by tamoxifen (OHT indicated by uppermost black bars) for reprogramming astrocytes into neurons.

(legend continued on next page)



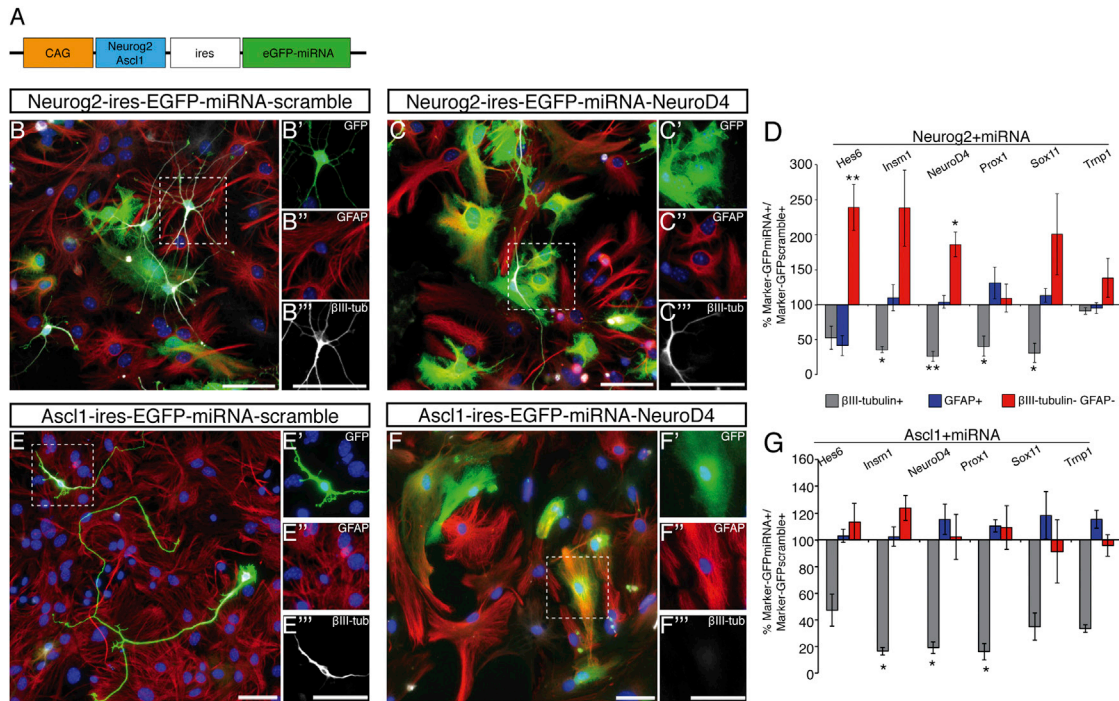


**Figure 2. Identification of Essential Downstream Effectors in Astrocyte Reprogramming**

(A) Schematic representation of retrovirus with expression cassette for miRNAs.

(B, C, E, and F) Micrographs of astrocytes, infected with the vectors indicated on top of the panels (green), were immunostained for GFAP (red) and  $\beta$ III-tubulin (white). Scale bars, 50  $\mu$ m.

(D and G) Quantification of changes in  $\beta$ III-tubulin+ neurons (gray bars), GFAP+ astrocytes (blue bars) or double-negative cells (red bars) at 8 DPI with the vectors indicated on top of the histograms. Mean  $\pm$  SEM in (D); n = 4 independent experiments (\*p < 0.05; \*\*p < 0.01). Mean  $\pm$  SEM in (G); n = 3 independent experiments (\*p < 0.05).

See also Figure S2.

Ascl1ERT2 were validated by real-time qPCR at 24 hr (Figures 1K and 1L). The expression of *Dlx2*, a known target of Ascl1 (Poitras et al., 2007), was unaffected by Neurog2ERT2 (Figure 1K), and expression of *Phf6*, a Neurog2-regulated gene (Voss et al., 2007), was reduced after Ascl1ERT2 activation (Figure 1L), confirming that the overexpression of these factors in astrocytes did not affect their target specificity.

### Identification of Target Genes Crucial for the Reprogramming of Astroglial Cells

To examine the contribution of the common downstream targets during reprogramming, we designed miRNAs against a subset of these candidates (most efficient in red; Figure S2). While astrocytes transduced with a construct co-expressing Neurog2 and

a miRNA-scramble control gave rise to a substantial number of  $\beta$ III-tubulin+ neurons (Figures 2A and 2B–2B''), much fewer neurons were generated upon a specific miRNA's co-expression (Figures 2C–2C'''; example with miRNA-NeuroD4). All Neurog2-IRES-miRNA constructs except for Neurog2-IRES-miRNA-Trnp1 reduced the proportion of neurons among infected cells to almost 50% or less compared to Neurog2-miRNA-scramble control (Figure 2D). The percentage of GFAP+ cells did not change significantly between gene-specific and scramble-miRNAs (Figure 2D) with the exceptions of miRNA-Hes6 and miRNA-Prox1. Upon knockdown of *Hes6*, *Insm1*, and *NeuroD4*, the proportion of GFAP- $\beta$ III-tubulin double negative cells increased among GFP-labeled cells (Figure 2D), suggesting that some transduced cells might have undergone partial reprogramming.

(B, C, E, and F) Micrographs of astrocytes infected with the constructs indicated in red on the left side and immunostained for the astrocytic marker GFAP (green) and the neuronal marker  $\beta$ III-tubulin (white). Scale bars, 100  $\mu$ m.

(D and G) Quantification of non-reprogrammed cells (GFAP) or reprogrammed cells ( $\beta$ III-tubulin) without or with OHT 8 days post-induction (DPI). Mean  $\pm$  SEM; n = 4 independent experiments; statistical test: two-tailed Mann-Whitney test (\*p < 0.05).

(H) Schematic representation of the experimental procedure for genome-wide mRNA analysis.

(I) Heatmap of genes regulated by both Neurog2ERT2 and Ascl1ERT2 within 24 hr after induction by OHT.

(J) Venn diagram of genes regulated by Neurog2ERT2 or Ascl1ERT2 24 hr after OHT.

(K and L) Real-time qPCR analysis on selected candidates upon Neurog2ERT2 (K) or Ascl1ERT2 (L) induction by OHT for 24 hr. Mean  $\pm$  SEM; n = 3 independent experiments.

See also Figure S1, Table S1, Table S2, Table S3, Table S4, and Table S5.

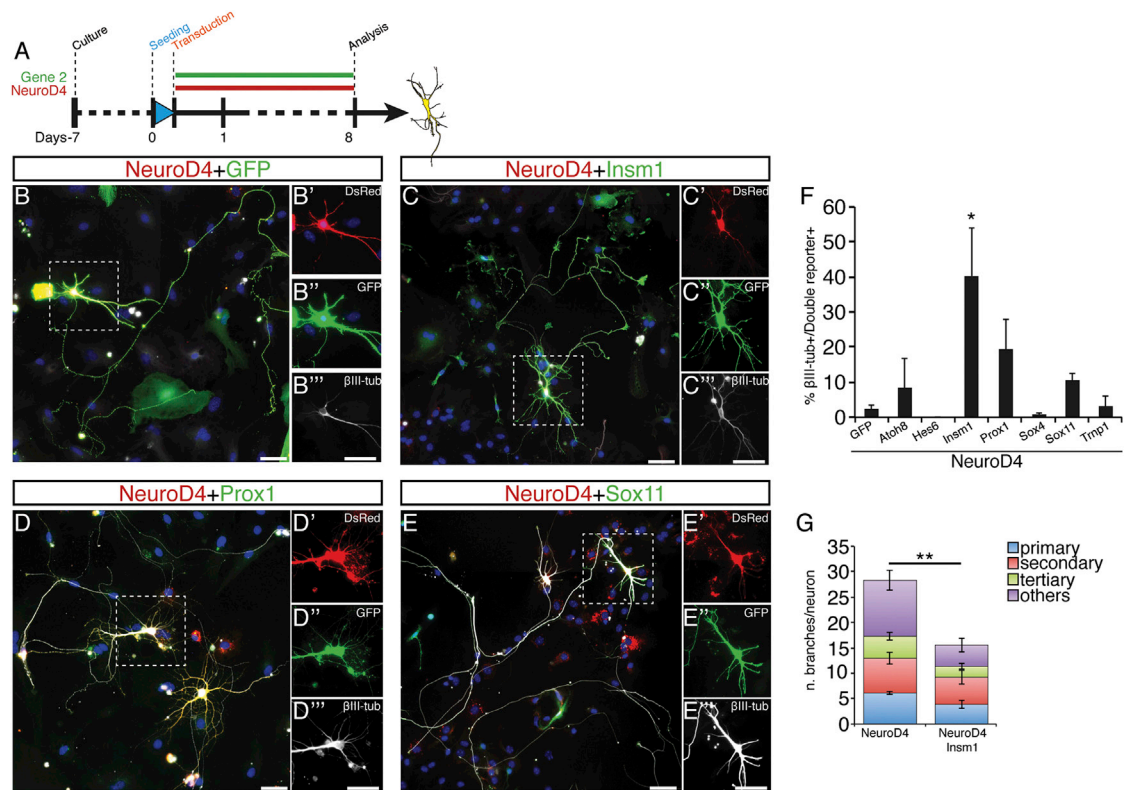


### Figure 3. Combinations of Common Downstream Targets Reprogram Astrocytes into Neurons

(A) Schematic representation of the experimental procedure.

(B–E) Micrographs depicting astrocytes co-infected with the constructs indicated on top of the panels (red and green) immunostained for  $\beta$ III-tubulin (white) at 8 DPI. Scale bars, 50  $\mu$ m.

(F) Quantification of  $\beta$ III-tubulin+ cells with neuronal morphology among DsRed+GFP+ double infected cells at 8 DPI. Mean  $\pm$  SEM; n = 4 independent experiments (\*p < 0.05).

(G) Quantification of branches per neurons/combination. Mean  $\pm$  SEM; n = 3 independent experiments (\*\*p < 0.01).

See also Figures S3 and S4.

Consistent with the selected factors acting also downstream of *Ascl1*, miRNAs against *Insm1*, *NeuroD4*, and *Prox1* reduced the proportion of neurons induced by *Ascl1* in astrocytic cultures to 20% or less of the proportion of neurons found in *Ascl1*-miRNA-scrambled-transduced cultures and to 50% or less for *Hes6*, *Sox11*, and *Trnp1* (Figures 2E–2E''' and F–F''', quantification in Figure 2G). Little increase in GFAP+ or double negative cells was observed in cultures transduced with *Ascl1*-specific miRNA viruses (Figures 2E and 2G). Thus, *Ascl1* represses the astrocyte fate independently of the selected neurogenic targets, in contrast to *Neurog2* (Figure 2D).

Together these data indicate that few commonly regulated neurogenic transcription factors are essential contributors to the reprogramming process.

#### Direct Neuronal Reprogramming by Downstream Effectors

To test whether the selected downstream transcription factors could elicit neuronal reprogramming on their own, we combined the expression of three genes at time and found *NeuroD4* (ND4) present in all of the pools inducing neurons at 8 days post-transduction (DPT) (Figure S3A). Moreover, ND4 alone was sufficient

to induce a small but consistent fraction of  $\beta$ III-tubulin+ neuronal cells (1%–3%, Figures 3A and 3F), while none of the other factors succeeded in doing so (data not shown). With the combination of two factors, ND4 was most efficient in eliciting neuronal conversion with *Insm1* (I), *Prox1* (P), or *Sox11* (S11) (Figures 3C–3F). Reprogrammed cells showed a distinct neuronal morphology with elaborated dendrites and a long thin process, reminiscent of an axon (Figures 3B–3E). ND4-induced neurons had more branched neurites than *NeuroD4*-*Insm1*-induced neurons (ND4+I), suggesting that these might be distinct neuronal subtypes (Figure 3G).

To determine whether reprogrammed neuronal cells acquired a genuine neuronal identity, cells transduced with the most efficient combinations of target genes (ND4+I, ND4+P, and ND4 as control; Figures 4B–4D) were analyzed by patch-clamp recording at 28–35 DPI after a 2-week co-culture with cells derived from cerebral cortex at embryonic day (E)14.5 (Figure 4A). All cells with neuronal morphology recorded upon ND4 expression (17/17, Figure 4B, n = 5 independent experiments) or ND4+I (11/11, Figure 4C, n = 3) generated action potentials (APs) upon receiving an injection of suprathreshold current pulses, whereas only 45.5% (5/11, Figure 4D, n = 2) of ND4+P

co-transduced neurons fired an AP. Analysis of neuronal properties, such as resting membrane potential, input resistance, somatic membrane time constant, AP threshold, and mean AP amplitude (summarized in Figure 4E) confirmed the functional neuronal nature of reprogrammed cells. ND4-transduced neurons responded to injection of suprathreshold current pulses (1 s) with repetitive spike discharges (example in Figure 4B''') associated with frequency adaptation in 72% of cases (8/11, Figures 4B'' and 4B'''), as did ND4+I neurons (6/6; example in Figure 4C'' and 4C''') and ND4+P neurons (5/5, Figures 4D'' and 4D'''); for higher variability see pie chart in Figure 4D'''). Interestingly, this pattern resembles that of regular spiking neurons recorded in acute slices of the cerebral cortex (Zolles et al., 2009).

As proof of principle, ND4-reprogrammed neurons were recorded during pharmacological treatments: for instance, addition of TTX (0.5  $\mu$ M,  $n = 3$ ) to the bathing solution reversibly blocked the spike induction in ND4 cells (Figure S3B), suggesting that the APs were generated by the activation of voltage-dependent Na<sup>+</sup> channels. Moreover, all cells received strong spontaneous synaptic input (Figure S3C, left graphs), either GABAergic, as hyperpolarizing potentials or outward currents recorded under voltage-clamp conditions at  $-60$ mV could be as reversibly inhibited by the GABA<sub>A</sub> receptor antagonist bicuculline (10  $\mu$ M) (Figure S3C, middle trace), or glutamatergic, as revealed by reversible blockage by the AMPA-receptor antagonist NBQX (10  $\mu$ M) (Figure S3C, right trace).

As the above data demonstrate that reprogrammed neurons receive functional synapses, we next examined whether they were also competent to form synapses by recording ND4 or ND4+I reprogrammed neurons in the absence of (E)14.5 primary neuronal co-cultures. Already at 8 DPT both ND4 and ND4+I neurons were able to form functional synapses as indicated by the existence of autaptic responses. In ND4-induced neurons, step-depolarizations during voltage-clamp recordings to membrane potentials of  $-10$ mV to  $0$ mV elicited autaptic currents (2/11 neurons recorded), which were blocked by NBQX (5–10  $\mu$ M), thus indicating that these autaptic responses were mediated by synaptically released glutamate via the AMPA-receptor (Figure 4F). Of 12 ND4+I-induced neurons tested, 8 showed autaptic responses that were in all tested cases (5/5) glutamatergic, as they were suppressed by NBQX (5–10  $\mu$ M; reversible after a prolonged washout period,  $n = 1$ , Figure 4G) but not by the GABA<sub>A</sub> receptor antagonist bicuculline ( $n = 4$ ). In agreement with electrophysiological data, ND4+I neurons were immunopositive for the synaptic vesicular glutamate transporter vGluT1 (Figure 4H). Thus, the common factors ND4+I induce a glutamatergic neuronal phenotype from cerebral cortex astrocytes.

### NeuroD4 and Insm1 Reprogram Murine Fibroblasts and Human Astrocytes

To determine whether the identified combinations of downstream proneural targets also have a reprogramming activity in other cell types, we expressed them in mouse embryonic fibroblasts (MEFs) (Vierbuchen et al., 2010) and human astrocyte cultures (same cells as in Guo et al., 2014). In MEFs, only ND4+I generated  $\beta$ III-tubulin<sup>+</sup> cells at 14 DPT (Figures S4A–S4D, quantification in Figure S4E), while ND4 alone (Figure S4C) or in combination with other targets failed to do so (data not shown). In human astro-

cyte cultures (Figures S4F and S4G'),  $\beta$ III-tubulin<sup>+</sup> cells appeared in samples transduced with ND4 alone or in combination with the selected genes already at 8 DPT (Figures S4I–S4L, quantification in M), but not in control cells (Figure S4H). Thus, these downstream transcription factors are also sufficient to reprogram cells from other species or germ layers.

### Astroglia Reprogramming Is Impaired when Neurog2ERT2 Activation Is Delayed

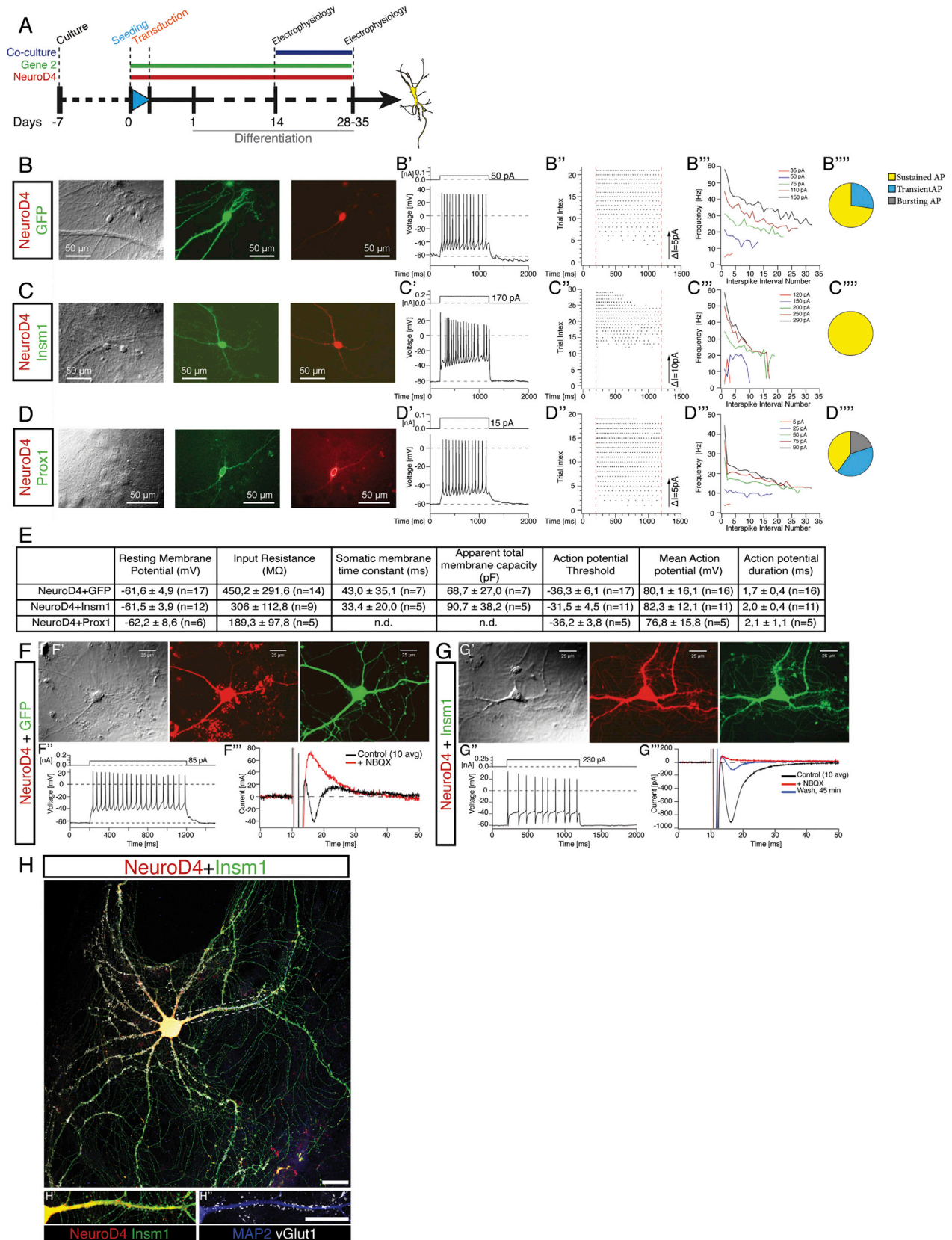
As astrocytes at postnatal stages are still plastic and proliferate (Ge et al., 2012; Laywell et al., 2000), we tested how reprogramming would be affected if astrocytes were cultured for a longer time. To this end, we maintained Neurog2ERT2-transduced murine astroglial cells in culture for 6 or 8 extra days (data not shown) before starting OHT treatment for 6 days (Figure 5A; condition is referred to as “delayed induction” or prolonged culture [6 days after passaging], while the condition described in Figure 1A is referred to as “early induction” [1–2 days after passaging]). Similar to the untreated controls (Figures 5B and 5D), very few neurons appeared in OHT-treated Neurog2ERT2-transduced prolonged cultures (Figures 5C and 5D) with the majority of them still expressing GFAP and maintaining astroglial morphology. Likewise, delayed induction of *Ascl1ERT2* also impaired reprogramming significantly, albeit less dramatically than for Neurog2ERT2 (data not shown). Therefore, prolonged culture of astrocytes renders them more resistant to proneural factor-induced reprogramming, which is similar to previous results obtained by multiple passages of astrocyte cultures (Price et al., 2014).

The expression of the selected downstream targets was examined after delayed induction, and *NeuroD4* was the only target still upregulated by Neurog2ERT2, albeit 5-fold less than it was after early activation of Neurog2ERT2 (Figure 5E). ChIP-qPCR on early OHT-treated Neurog2ERT2-transduced cells revealed that Neurog2ERT2 was significantly enriched at several of its downstream targets (*Atoh8*, *Insm1*, *NeuroD1*, *NeuroD4*, *Prox1*, *Sox11*, and *Trnp1*; Figure 5F, ChIP early), indicating that Neurog2ERT2 directly activates these targets in astroglia by binding to their regulatory elements. However, with the delayed induction protocol, Neurog2ERT2 was bound less to *NeuroD1*, *NeuroD4*, and *Trnp1* promoters (Figure 5F), which is statistically not different from the negative control region (DII1 ORF). Thus, astroglial cells in culture are not in a stable permissive state for reprogramming but they become increasingly refractory to conversion into neurons, a process that might involve a reduced accessibility of Neurog2 to target genes important for the reprogramming process.

### Selected Target Genes Downstream of Neurog2 and Ascl1 Induce Reprogramming of Prolonged Astroglia Cultures

If the failure of target gene activation is responsible for the low reprogramming efficiency in the prolonged cultures, this should be overcome by expression of these targets (Figure 5G). Indeed, in cultures maintained for a longer time, combinations of ND4 with *Insm1*, *Prox1*, or *Sox11* elicited the generation of neuronal cells (Figures 5I and 5J) more efficiently than ND4 alone (Figures 5H and 5K). Likewise, combining *Neurog2ERT2* with *Insm1*,





(legend on next page)



*NeuroD4*, *Prox1*, or *Sox11* led to neuronal reprogramming also in prolonged cultures, while cells co-transduced with Neurog2ERT2 and a control virus largely remained astroglia (Figures S5A–S5E, quantification in Figure S5F).

Thus, impairment in neuronal reprogramming in prolonged astroglial cultures is due to a failure in the activation of these common neurogenic fate determinants while the underlying downstream neurogenic program is still amenable for activation.

### REST Represses *NeuroD4* Transcription in Competition with *Neurog2*

The reduced Neurog2ERT2 binding to target loci upon delayed activation suggested that changes in the chromatin state might take place at these target loci (see Hirabayashi and Gotoh, 2010 for review). We focused on *NeuroD4* as one of the main target genes mediating the reprogramming activity of Neurog2 and *Ascl1* in astroglial cells. Between the cultures collected at different time points, we did not observe any significant change in the repressive marks H3K27me3 and 5mC or the active mark H3K4me3 analyzed by ChIP-qPCR at several locations in this gene, including the Neurog2ERT2-bound enhancer, intron, and promoters (Figures S6A–S6E), while H4K20me3 was enriched in prolonged cultured astrocytes compared to short-term cultures (Figures 6A and 6A'). These data suggest that remodeling of the chromatin at *NeuroD4* locus occurred over time such that it became more heterochromatin-like (Wongtawan et al., 2011).

As a repressor complex might be involved in such a change, we focused on REST, known to repress neuronal gene expression in non-neural cells (Jørgensen et al., 2009). By ChIP-qPCR, REST was confirmed to be present at the *NeuroD1/4* loci in astroglial cells soon after plating (Figures 6B and 6B') (Gao et al., 2011; Johnson et al., 2008). REST ChIP following early activation of Neurog2ERT2 showed significantly reduced binding onto the *NeuroD4* promoter and less so on the *NeuroD1* or *Sox11* promoters (Figures 6C and 6C'). In contrast, Neurog2ERT2 delayed activation had no effect on REST binding (Figures 6C and 6C'), suggesting that the proneural factor Neurog2 and REST can compete for binding at this site in early cultures, but no longer at later stages. Importantly, western blot analysis revealed that REST protein level was unchanged over

time (Figures S6F–S6F'), thus excluding the possibility that Neurog2 could compete with REST early on but not late because of a higher abundance of REST protein in prolonged cultures.

To directly investigate the role of REST in preventing astroglia reprogramming in prolonged cultures, we generated astroglia cultures from P6 cerebral cortex of mice homozygotes for a new conditional allele of REST (hereafter referred to as REST<sup>fllox</sup>, see Experimental Procedures and Figure S6G) and transduced them with a Cre-recombinase-encoding adenovirus either immediately after passaging the astrocytes or with a 5 day delay. In both conditions, REST protein disappeared within 48 hr (Figures S6H–S6H', black arrow). As Cre-mediated recombination removes exon 2 (Figure S6G) and a truncated form appeared in the western blot (Figure S6H', empty arrow), we verified that this truncated form has no binding capability (i.e., no significant difference in enrichment between REST-ChIP and mock-ChIP samples, and 5- to 10-fold reduced binding capability compared to REST-expressing astrocytes; Figure S6I, and for comparison, Figure 6B). Thus, Cre-mediated deletion of exon 2 generates a truncated form of REST unable to bind to DNA. Upon REST deletion in short-term cultures, both *NeuroD1* (Gao et al., 2011) and *NeuroD4* were upregulated, while REST ablation in prolonged cultures had no significant effect on *NeuroD1* or *NeuroD4* expression (Figures S6J–S6J').

To test whether REST could prevent Neurog2ERT2 from binding to the *NeuroD4* promoter in astrocytes cultured for 6 days (Figure 6D), we co-infected the cultures with Cre and Neurog2ERT2, thus deleting REST from the beginning of the culture, and initiated OHT treatment 6 days later. ChIP-qPCR revealed a significant increase of Neurog2ERT2 onto *NeuroD4* promoter compared to REST-expressing cells, with a small effect on Neurog2ERT2 binding to *Atoh8* and *NeuroD1* loci (Figure 6D'). In these conditions (early REST deletion and delayed Neurog2ERT2 activation, Figure 6E), *NeuroD4* and *Tmp1* were upregulated (Figure 6E', gray bars). However, when REST was removed 5 days after Neurog2ERT2 transduction (Figures 6E and 6E'), *NeuroD4* was not upregulated after Neurog2ERT2 delayed activation (Figure 6E', black bars).

Together, these data suggest that *NeuroD4* becomes less prone to activation over time, likely through the initial transient

### Figure 4. Generation of Synaptically Mature Neurons upon Combined Expression of Downstream Targets

(A) Schematic representation of the experimental procedure.

(B–D) Electrophysiological characterization of induced neurons upon overexpression of the constructs indicated by live fluorescence during recordings. Examples of sustained trains of APs generated when recording in current-clamp mode are shown (in B', C', and D' top panel: stimulation protocol). 50% repetitive firing *NeuroD4*/GFP cells present first spike latency lower than 70 ms, with 50% higher than 150 ms; an example of frequency adaptation is shown (B'' and B'''). In (C'), an example of a repetitive AP generated in *NeuroD4*/Insm1 transduced cells is shown (four generated the first spike with a latency lower than 70 ms and the remaining two did so with a latency higher than 150 ms) and characterized by spike accommodation (C'') and spike adaptation (C'''). (D'' and D''') show examples of repetitive spike discharge in *NeuroD4*+*Prox1*-expressing neurons. (B''''–D''''') A pie chart shows the fraction of cells firing bursting (gray), transient (blue), or sustained (yellow) APs.

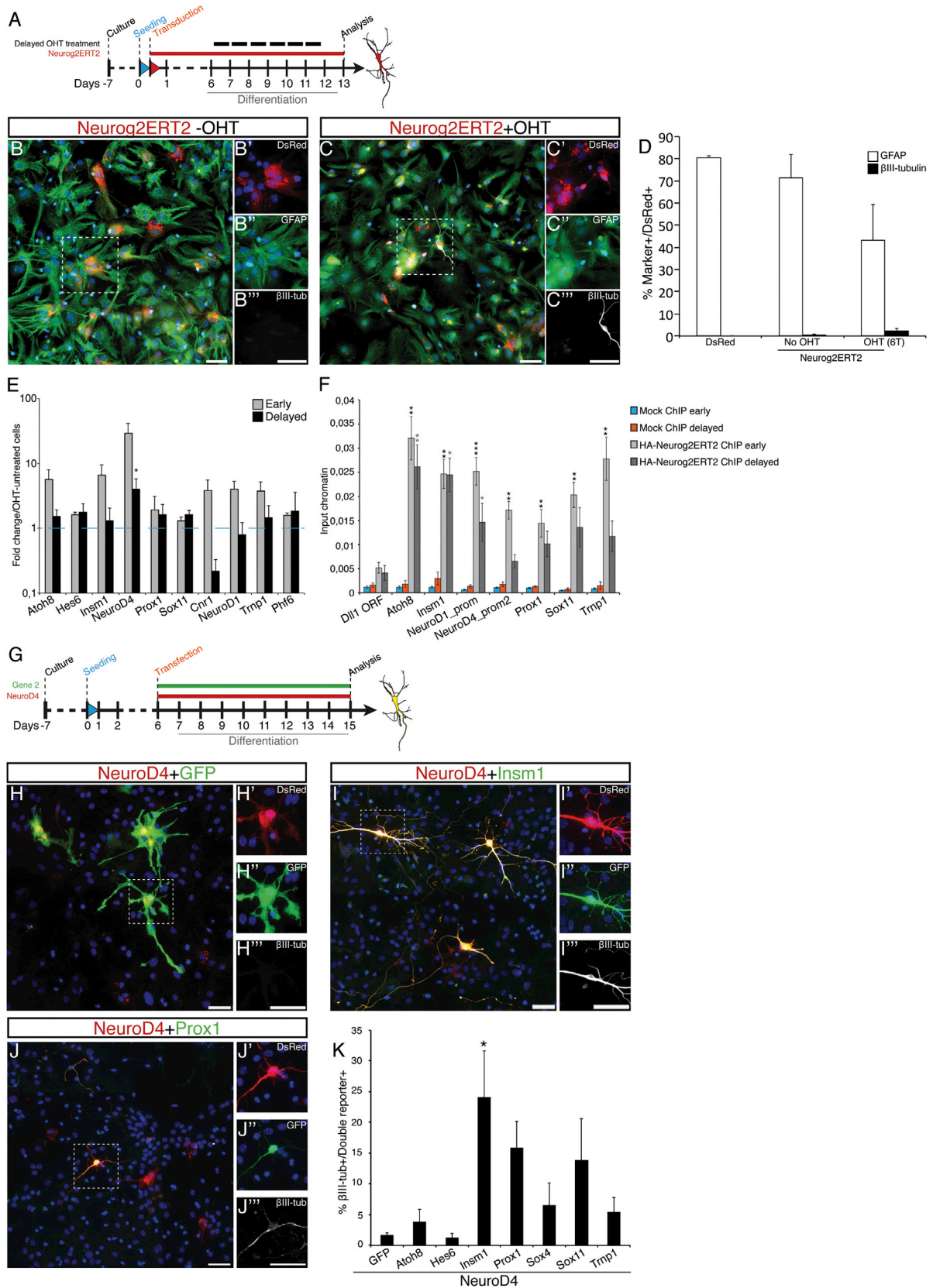
(E) Table summarizing the electrophysiological parameters measured (brackets indicate the number of cells analyzed).

(F) Example of *NeuroD4*-induced neurons at 14 DPT (F'). A depolarizing current pulse (1 s, 85 pA) induced a train of APs (F''). In (F''') the autaptic response (black trace, average of 10) could be blocked by NBQX (5  $\mu$ M, red trace, average of 10).

(G and G') Example of *NeuroD4*-*Insm1*-induced neurons at 14 DPI. A depolarizing current pulse (1 s, 230 pA) induced a train of APs (G''). In (G''') the autaptic responses (black trace, average of 10) could be blocked by NBQX (10  $\mu$ M, 10 min red trace, average of 10) and partially reversed following washout for 45 min (blue trace).

(H) Micrograph depicting a neuron induced by co-expression of *NeuroD4*-containing viral vector (red) and *Insm1*-containing viral vector (green) immunostained at 30 DPI for MAP2 (H', blue) and vGlut1 (H'', white). Scale bar, 50  $\mu$ m.

See also Figure S3.



(legend on next page)

repressor activity of REST followed by a histone modification that makes the locus more compact.

### REST Deletion Alleviates the Reprogramming Blockage in Prolonged Astrocytic Cultures

To examine the effect of REST deletion on Neurog2ERT2-dependent neuronal conversion, REST<sup>fllox</sup> astrocytes were co-infected with Neurog2ERT2- and Cre-encoding viruses soon after being plated, or with a 5 day delay (Figure 7A). Cultures were then treated for 3 consecutive days with OHT and analyzed 8 DPI (Figures 7B–7E, Figures S7A–S7D). As previously reported (Xue et al., 2013), REST deletion generated a fraction of  $\beta$ III-tubulin+ cells on its own without Neurog2ERT2 activation (around 20%, Figure 7F); strikingly, however, 90% of Cre/Neurog2ERT2 transduced cells were  $\beta$ III-tubulin+ after early REST deletion and delayed Neurog2ERT2 activation (Figure 7D). Delayed Cre-mediated REST deletion still allowed 50% of Cre/Neurog2ERT2 double positive cells to convert into  $\beta$ III-tubulin+ neurons after induction (Figure 7D), suggesting that other mechanisms are gradually taking over to block reprogramming.

Thus, REST is a key factor in silencing main neurogenic targets of proneural factors such that they are no longer accessible for reprogramming in astrocytes in prolonged cultures.

## DISCUSSION

The present study unraveled the transcriptional events taking place in the initial phases of astrocytes converting into neurons. This conversion occurred swiftly, in a dynamic manner, and with very distinct transcriptional programs between the proneural factors *Ascl1* and *Neurog2*. Thus, even within the same cell type from the same brain region maintained in the same environment, forced induction of glutamatergic and GABAergic neuronal fate follows essentially distinct paths, with relatively few genes common to both neurogenic cascades. The analysis of the identified shared target genes led us to identify a particularly important subset of downstream targets capable, when combined, of directly reprogramming astrocytes into functional neurons. Among these, *NeuroD4* seems instrumental to force direct reprogramming, and investigating the failure of *NeuroD4* induction in reprogramming-resistant astrocytes led us to uncover an important mechanism of chromatin accessibility control at the *NeuroD4* locus. Indeed, the binding of REST close to the *NeuroD4* promoter prevents the recruitment of *Neurog2*, while

accumulation of H4K20me3 occurred over time. Therefore, this work sheds light on some of the earliest mechanisms decreasing astrocyte reprogramming into neurons.

### Similarities and Differences between Gene Regulation in Development and Direct Reprogramming

Activation of Neurog2ERT2 or *Ascl1*ERT2 in astroglia cells revealed a highly dynamic regulation of gene expression within the first 48 hr of direct reprogramming: only a small subset of genes (7% and 13.5% for *Neurog2* and *Ascl1*, respectively) was regulated at least at two time points (Figures S1P and S1P'), suggesting a fast and hierarchical sequence of gene regulation. About one-third (188 out of 626) of the genes regulated by Neurog2ERT2 at any time in our analysis are common to the genes regulated by *Neurog2* in the developing cerebral cortex in vivo (Gohlke et al., 2008), and similar results were obtained by comparing *Ascl1*ERT2-regulated genes with *Ascl1*-electroporated cells in vivo (527 out of 1,669; Gohlke et al., 2008). The proportion of commonly regulated genes is rather low (18% at 48 hr, Figures S7E and S7F) when compared to *Ascl1*-regulated genes in neuronal reprogramming of MEFs (Wapinski et al., 2013). However, this expression analysis was performed at 48 hr with tetracycline-inducible cells, and, given the fast dynamic regulation of targets observed here, we can only conclude that at least some common target genes are activated during reprogramming of cultured MEFs or astrocytes (Table S7). These are enriched for neuronal differentiation and axon-related genes (Figure S7G, Table S7), such as *Dll3*, *Dcx*, neurofilaments, and the known targets *Dlx2/3*. *Hes6* was the only gene present in all the transcriptome data examined (Neurog2ERT2, *Ascl1*ERT2, in vivo *Neurog2*, *Ascl1* gain-of-function, *Neurog2* loss-of-function (Gohlke et al., 2008), and *Ascl1* in MEFs (Wapinski et al., 2013)) with 14 genes present in at least five different analyses (*Arl4A*, *Coro2B*, *Cxadr*, *Dll3*, *Efh2*, *Gpm6B*, *Hes5*, *Homer2*, *Isl1*, *Lrrc17*, *Plk3*, *Rgs16*, and *Shf*). Thus, even in very different cell types at different developmental stages, some common target genes regulated by these proneural factors emerge.

### Identification of Common Neurogenic Factors

Among the genes regulated by *Neurog2* and *Ascl1* in astrocyte reprogramming, many are pan-neuronal, such as *Elavl2*, synuclein a (*Snca*), neuronal pentraxin (*Nptx1*), *D11Bwg0517e* (*Rfox3*, also known as NeuN), and  $\beta$ III-tubulin (*tubb3*), as well as several key neurogenic transcription factors widely expressed in

### Figure 5. Delayed Induction of Neurog2ERT2 Reveals a Block in Astrocyte Reprogramming

(A) Scheme of the experimental procedure.

(B and C) Micrographs of Neurog2ERT2-infected astrocytes (red) immunostained for GFAP (green) and  $\beta$ III-tubulin (white), without (B) or with (C) OHT treatment starting at 6 days after being plated. Scale bars, 100  $\mu$ m.

(D) Histogram depicting the proportion of GFAP+ or  $\beta$ III-tubulin+ cells among infected cells upon delayed Neurog2ERT2 activation at 13 DPI. n = 4 independent experiments.

(E and F) Histograms of real-time qPCR (E) and HA-Neurog2ERT2  $\mu$ ChIP-PCR (F) of astrocyte cultures treated as indicated in the legend (early, early OHT treatment, gray bars in E from Figure 1A; and delayed, OHT treatment 6 days later). For (F) cells were exposed to OHT treatment for 24 hr. Percentages of input chromatin were quantified in duplicate from three independent biological samples (mean  $\pm$  SEM). Significance was tested between samples and respective *Dll1* ORF negative region by two-tailed unpaired t test (\*p < 0.05, \*\*p < 0.01, \*\*\*p < 0.0001).

(G) Scheme of the experiment.

(H–J) Micrographs of astrocytes transfected with the constructs indicated on top of the panels with a 5 day delay immune-stained for  $\beta$ III-tubulin 8 days post transfection (DPT). Scale bars, 50  $\mu$ m.

(K) Histogram depicting the proportion of  $\beta$ III-tubulin+ cells at 8 DPT. Mean  $\pm$  SEM; n = 4 independent experiments (\*p < 0.05).

See also Figure S5.

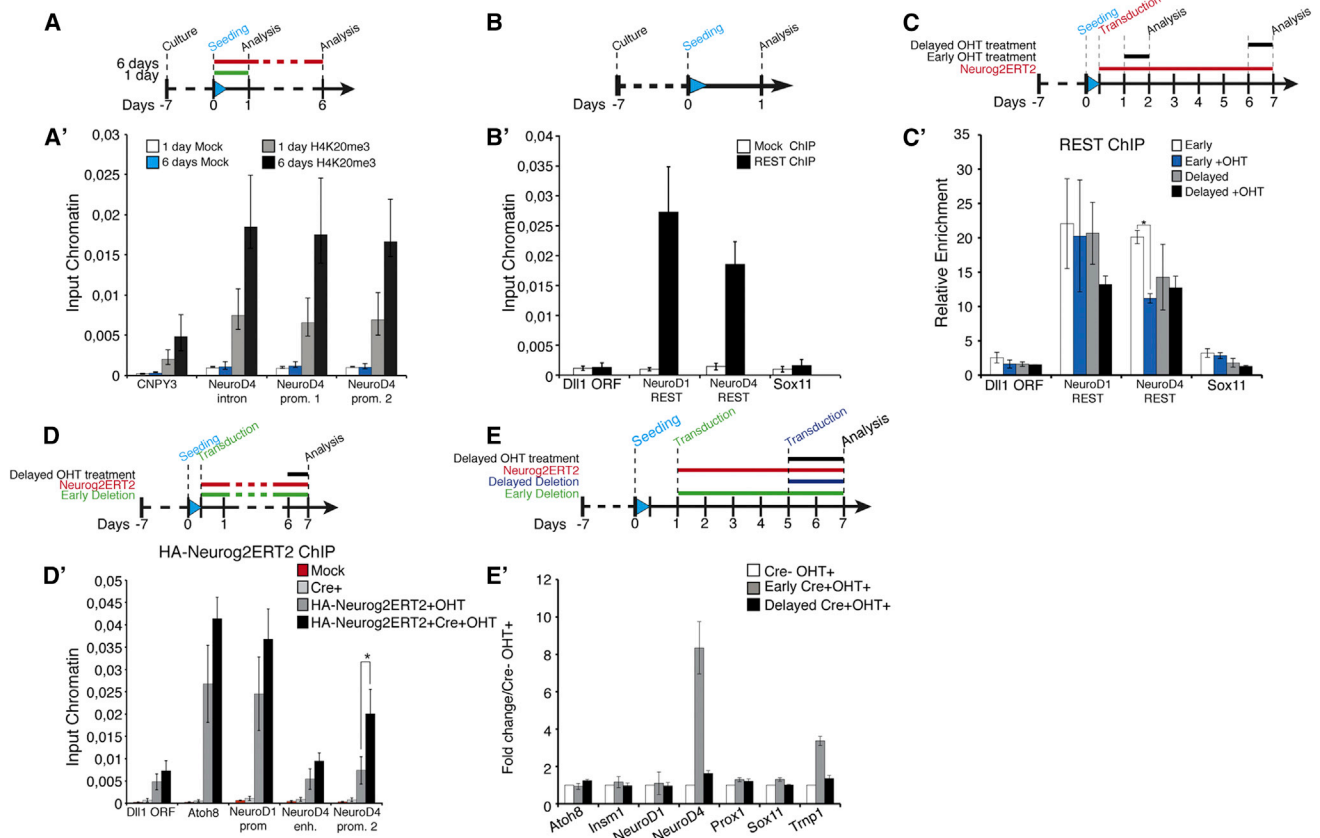


**Figure 6. Chromatin Marks and REST Binding at Regulatory Regions of the Downstream Targets NeuroD4, NeuroD1, and Sox11**

(A and A') H4K20me3  $\mu$ ChIP-PCR on immunoprecipitated material from astroglia cultures collected 1 day or 6 days after being plated as indicated in the scheme at top of (A).

(B and B') Analysis of REST binding to *NeuroD4* by  $\mu$ ChIP-PCR on immunoprecipitated samples from short-term astroglia cultures as indicated in the scheme in (B). Amplification of the REST binding element within the *NeuroD1* intron was used as a positive control while a region within the promoter of *Sox11* was used as a negative control. Percentages of input chromatin were quantified in duplicate from three independent biological samples (mean  $\pm$  SEM).

(C and C') REST  $\mu$ ChIP-PCR on immunoprecipitated samples from Neurog2ERT2-transduced astrocytes cultured for shorter or longer periods and treated with OHT for 24 hr as indicated at the top of (C). REST ChIP values were normalized to their respective mock ChIP values (mean  $\pm$  SEM in duplicate from three independent biological samples; two-tailed unpaired t test, \* $p < 0.05$ ).

(D and D') HA-Neurog2ERT2  $\mu$ ChIP-PCR on immunoprecipitated genomic DNA from delayed astroglia cultures. RESTflox cKO were transduced with Neurog2ERT2 and adeno-Cre virus with a late OHT induction as indicated (D). The *Atoh8* promoter and *NeuroD1* promoter regions were used as controls for the effect of REST deletion on Neurog2 binding. Percentages of input chromatin were quantified in duplicate from three independent biological samples (mean  $\pm$  SEM; two-tailed unpaired t test, \* $p < 0.05$ ).

(E and E') Real-time qPCR analysis on Neurog2ERT2-astrocytes treated with OHT for 48 hr after early or late REST Cre-mediated deletion as indicated at the top of the histogram (E). Control samples (Cre- OHT+) were transduced with adeno null virus 1 day after being seeded at the same time as the delayed Cre sample (adeno-Cre virus, Early Cre+OHT+). In parallel, another set of cells was transduced with adeno-Cre virus 5 days later (Delayed Cre+OHT+). Mean  $\pm$  SEM in duplicate from three independent culture batches.

See also Figure S6.

neurogenesis, reflecting their implication in many different neuronal lineages (Figure 1H, Table S6).

Loss-of-function studies on the common downstream targets revealed their crucial role in mediating Neurog2- and *Ascl1*-induced reprogramming (Figure 2). Interestingly, most of the cells transduced with Neurog2 and specific miRNAs for these targets (*Hes6*, *Insm1*, *NeuroD4*, and *Sox11*) were negative for both the neuronal marker  $\beta$ III-tubulin and the astroglial marker GFAP (Figure 2D), suggesting that activation of these targets is not required to block the astroglial fate but rather to induce the neuronal fate. Conversely, the combination of just two of these

common neurogenic transcription factors is sufficient to trigger reprogramming of cells into functional neurons from both mouse astroglia (Figures 3, 4, and S3) and human astrocytes and MEFs (Figure S4), suggesting that the identified targets mediate critical biological processes required to induce the neuronal fate, such as transcriptional regulation and cytoskeleton reorganization.

Among the factors tested, *NeuroD4* was the only gene capable of reprogramming astrocytes into functional neurons on its own. However, only a minority of *NeuroD4*-induced neurons seem to complete synaptic maturation, while the co-expression of *Insm1* seems sufficient to allow them to reach a fully mature



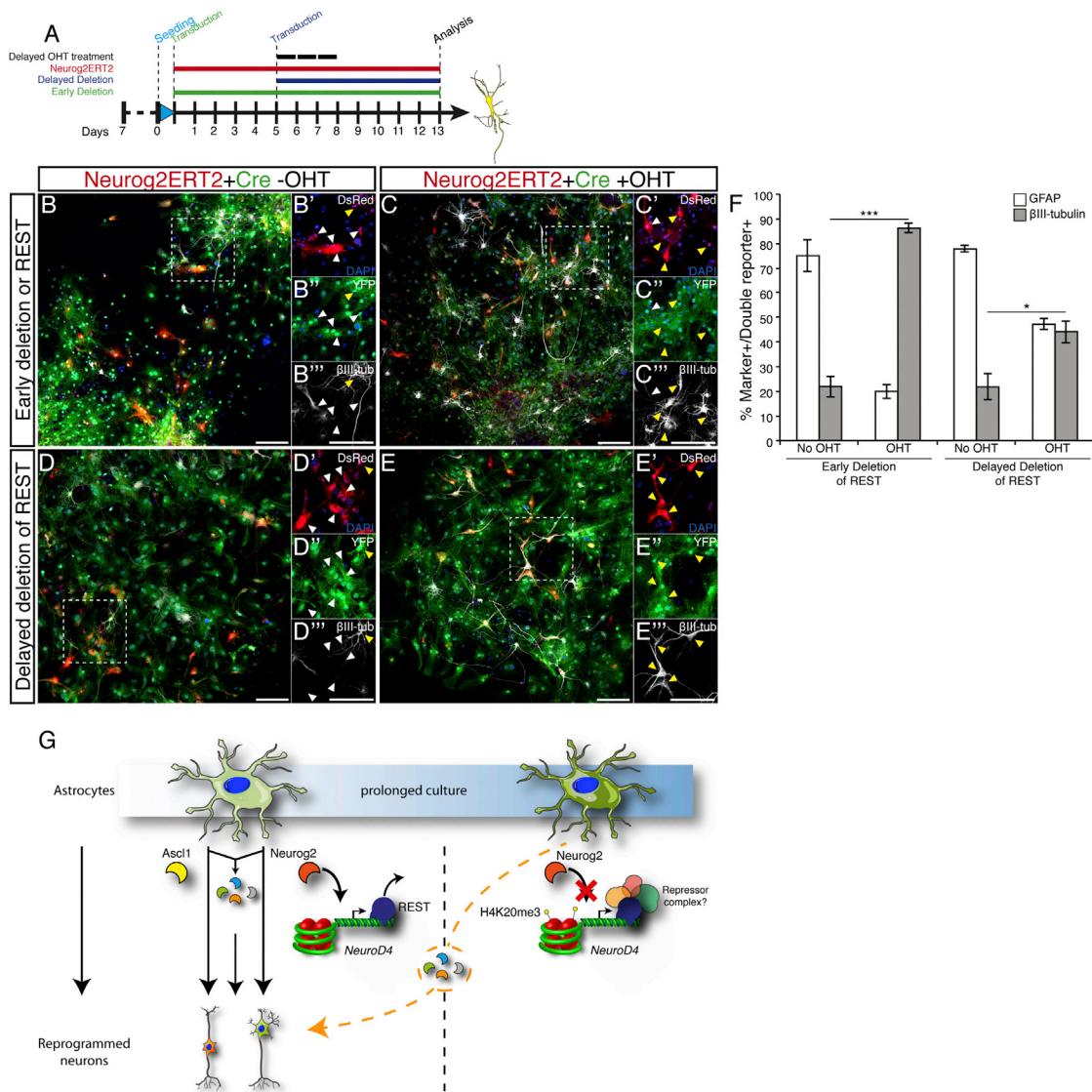


### Figure 7. Deletion of REST Removes Reprogramming Block in Astrocytes

(A) Schematic representation of the experimental procedure.

(B–E) Micrographs of Neurog2ERT2-infected astrocytes (red) with early (B and C) or late (D and E) deletion of REST by infection with a Cre containing viral vector (green) immunostained for the neuronal marker βIII-tubulin (white) at 8 DPI. Yellow arrowheads indicate triple positive cells (DsRed, YFP, βIII-tubulin) while white arrowheads indicate double positive cells (DsRed, GFP). Scale bars, 150 μm.

(F) Histogram depicting the proportion of co-transduced double positive cells (red and green) for the astrocytic marker (GFAP, white bars) or the neuronal marker (βIII-tubulin, black bars). Mean ± SEM, three independent biological samples; two-tailed unpaired t test, \*p < 0.05; \*\*\*p < 0.001.

(G) Postnatal (day 6–7) mouse cortical astrocytes transduced with Ascl1 or Neurog2 are reprogrammed into neurons. However, when cells are maintained longer in culture, increasing levels of H4K20me3 modify the local chromatin environment that becomes favorable to the repressive complex REST. Consequently, Neurog2 fails to access the NeuroD4 promoter. This is bypassed by common downstream transcription factors to both Ascl1 and Neurog2 that are able to generate neurons also in prolonged astrocytic cultures. Unidentified REST co-factors might be recruited to the locus to further remodel the chromatin over time. See also Figure S7.

synaptic glutamatergic phenotype. Thus, the NeuroD family of bHLH transcription factors (including also NeuroD1 and 2; Guo et al., 2014; Yoo et al., 2011) appears to be particularly important in neuronal reprogramming.

### REST Is a Critical Repressor of NeuroD4

When Neurog2ERT2-transduced astrocytes were maintained in culture for 6 days before OHT treatment, only a small fraction

of them converted into neurons, most likely as a consequence of the reduced induction of some targets, such as *NeuroD4* (Figure 4E), suggesting that within this short period of time reprogramming blocks were already established.

Examining the chromatin landscape changes at the *NeuroD4* locus, we detected an enrichment of the heterochromatin-associated histone mark H4K20me3 (Wongtawan et al., 2011) at the *NeuroD4* promoter in prolonged cultured cells, suggesting a

progressive reduction of chromatin accessibility at this locus. Interestingly, REST is highly enriched at both *NeuroD1* and *NeuroD4* loci initially but less at the *NeuroD4* promoter in astrocytes cultured for 6 more days (Figure 6C'), suggesting that REST is important in initiating the silencing of *NeuroD4*, but additional repressive mechanisms may be involved at later stages. Consistent with this hypothesis, the binding competition between Neurog2 and REST only occurred in cultures soon after they were plated (Figure 6C'), and a strong activation of *NeuroD4* in prolonged cultures occurred only upon early deletion of REST (Figure 6E). These observations thus revealed a temporal window during which REST binding/activity can be modulated.

REST ablation resulted in a striking improvement of reprogramming efficiency upon delayed Neurog2ERT2 activation when REST was deleted early but also when it was deleted late, thus suggesting important functions of REST-regulated genes other than *NeuroD4* in astrocyte reprogramming. Further studies will be required to examine the mechanism underlying the essential role of REST in orchestrating gene silencing in astrocytes (Figure 7G). In different cell types, recruitment of other factors, such as HP-1 or HDAC1, is important to further silence gene transcription. However, we did not observe a significant difference in HP-1 or HDAC1 binding to *NeuroD4* between short- and prolonged astroglia cultures (data not shown). REST has recently been implicated in PTB-regulated miRNA-based MEF reprogramming (Xue et al., 2013) and identification of specific co-factors/regulators needs to be explored in astrocytes.

Importantly, our results revealed a hierarchical mode of target gene blockage mediating alternative fates. While Neurog2 could no longer regulate some of its targets, such as *NeuroD4*, in prolonged cultures, the targets of *NeuroD4* are still accessible, since *NeuroD4* with or without an additional common factor could still mediate reprogramming as efficiently as in short-term cultured astrocytes. Thus, our data suggest a developmental hierarchy in shutting off genes of alternative fates, a novel concept in elucidating the hurdles for direct reprogramming.

## EXPERIMENTAL PROCEDURES

### Cell Cultures of Astroglia from the Postnatal Mouse Cerebral Cortex

Astrocytes were cultured as previously described (Heinrich et al., 2010; Heins et al., 2002). MEFs were isolated as described (Vierbuchen et al., 2010). Human astrocytes were purchased from ScienCell (cat. #1800) and expanded as described in the protocol. For details on cell culture see the Supplemental Experimental Procedures.

### Immunocytochemistry

Cells were fixed and stained as previously described (Heinrich et al., 2011). For details and antibodies used see the Supplemental Experimental Procedures.

### RNA Extraction and Real-Time qPCR

6 to 12 wells from 24-well plates were collected for each time point. Subsequently, RNA was extracted with the RNeasy Plus Micro Kit (QIAGEN) according to the manufacturer's instructions, and genomic DNA was removed. RNA was retro-transcribed with SuperScriptIII Reverse Transcriptase and Random Primers (Roche). Each cDNA sample was diluted 1:5 and 1  $\mu$ l was used for each quantitative real-time reaction. Real-time qPCR was performed on a LightCycler480 instrument (Roche) with the LightCycler Probe Master kit (Roche) and Monocolor Hydrolysis Probe (UPL) Probe (Roche) according to the manufacturer's instructions (20  $\mu$ l final volume). The expression of each gene was analyzed in triplicate. Data were processed with the  $\Delta\Delta$ Ct method

(Livak and Schmittgen, 2001). Quantification was performed on three independent samples. Primers and probes are listed in the Supplemental Experimental Procedures.

### Microarray Analysis

10  $\mu$ g of amplified antisense RNA (aRNA) was hybridized on Affymetrix Mouse Genome 430 2.0 arrays containing about 45,000 probesets. Staining and scanning was done according to the Affymetrix expression protocol. GO term analysis was performed using DAVID (<http://david.abcc.ncifcrf.gov>). For details see Supplemental Experimental Procedures.

### Plasmids and DNA constructs

cDNA of selected genes was subcloned into self-inactivating retroviral vectors containing the actin promoter with cytomegalovirus enhancer (pCAG) driving the expression of the genes of interest linked to a fluorescent reporter through internal ribosomal entry site (IRES) as previously described (Heinrich et al., 2011). Flag-HA-Ascl1ERT2 and Flag-HA-Neurog2ERT2 were obtained by a fusion of the transcription factor cDNA together with the ERT2 domain of the estrogen receptor. For ChIP experiments, DsRed cDNA present in pCAG-Neurog2ERT2-IRES-DsRed was replaced with Puromycin cDNA to allow cell selection in the culture. For details see the Supplemental Experimental Procedures.

### Micro-ChIP and qPCR

Around 100,000 cells per sample were used for micro-ChIP ( $\mu$ ChIP). For details see the Supplemental Experimental Procedures.

### Western Blot

Cells were washed three times with 1X cold PBS, lysed with urea buffer (8M urea, 1M thiourea, 0.5% [w/v] CHAPS, 50mM DTT, and 24mM spermine), scraped with a sterile disposable cell scraper (Costar), transferred to an Eppendorf tube, and centrifuged at 14,000 rpm at room temperature for 30 min. Equal amounts of protein were loaded onto polyacrilamide gels (Novex, Life Technologies) and blotted with anti-REST (1/200; Millipore, 07-579) or anti-LaminB (1/1000; Santa Cruz, sc-6216 and sc-6217).

### Patch-Clamp Recording

Whole-cell current-clamp recordings were made using an npj ELC-03XS amplifier (npj, Tamm, Germany), which allowed current-clamp recordings in bridge mode and voltage-clamp measurements. For further information, see the Supplemental Experimental Procedures.

### Conditional REST Mouse Line

Mouse ESCs targeted with the L1L2\_Bact\_P cassette were obtained from the Sanger EUCOMM project (clone EPD0105\_1\_E05, <http://www.informatics.jax.org/allele/key/609045>) and injected into blastocysts to generate heterozygous animals with loxP sites flanking the second exon of REST. Subsequent crossings with Rosa26-floxed stop-YFP reporter mice (Srinivas et al., 2001) were performed to generate a homozygous REST<sup>lox</sup>/R26YFP line. In order to remove the neo selection cassette from the REST locus, we crossed REST<sup>neoflox</sup> animals with the Flip recombinase mouse line. Experiments conducted with REST<sup>lox</sup> mice were performed in accordance with a UK Home Office Project License and approved by the local ethics committee. All animal procedures were carried out in accordance with the policies of the use of animals and human material of the EU and the institutional animal committees implementing them.

### ACCESSION NUMBERS

Array data have been submitted to GEO under the accession number GEO: GSE60389.

### SUPPLEMENTAL INFORMATION

Supplemental Information for this article includes seven figures, seven tables, and Supplemental Experimental Procedures and can be found with this article online at <http://dx.doi.org/10.1016/j.stem.2015.05.014>.

## AUTHOR CONTRIBUTIONS

G.M. collected samples for the microarrays, generated the constructs for gain-of-function and loss-of-function experiments in astrocytes, performed most of the reprogramming experiments on mouse and human astrocytes and MEFs, and analyzed the data. S.G. performed the experiments related to the molecular mechanisms, analyzed the reprogramming in REST<sup>fllox</sup> mice, and analyzed the data. G.M., S.G., B.B., F.G., and M.G. conceived the experimental procedures; G.M., S.G., F.G., and M.G. wrote the manuscript; D.D. generated the initial inducible constructs; H.F.J. generated the REST<sup>fllox</sup> line; M.I. and J.B. performed the microarrays and analyzed the microarray data; B.S. performed all of the patch-clamp recordings; and S.S. and F.T. analyzed RNA-seq results and compared them with the microarray results.

## ACKNOWLEDGMENTS

We are particularly grateful to Tatiana Simon-Ebert, Detlef Franzen, Ines Mühlhahn, Carmen Meyer, and Gabi Jäger for excellent technical support; Alexandra Lepier for the support in viral vector production; Sergio Gascon for discussions; and Emily Violette Baumgart for reading the manuscript. We thank Ismini Rozani and Chiara Galante for their assistance in cloning. We thank members of the Götz and Guillemot groups for their discussion and support. This work was supported by a project grant from the Wellcome Trust (WT091800MA) and a Grant-in-Aid from the Medical Research Council (U117570528) to F.G. and by grants from SPP1356 of the Deutsche Forschungsgemeinschaft (BE 4182/2-2; GO 640/9-2), the BMBF ("NewNeurons") (both to M.G. and B.B.), and the Advanced ERC grant ChroNeuroRepair GA No. 340793 (to M.G.).

Received: August 22, 2014

Revised: March 27, 2015

Accepted: May 27, 2015

Published: June 25, 2015

## REFERENCES

- Berninger, B., Costa, M.R., Koch, U., Schroeder, T., Sutor, B., Grothe, B., and Gotz, M. (2007). Functional properties of neurons derived from in vitro reprogrammed postnatal astroglia. *J. Neurosci.* *27*, 8654–8664.
- Gao, Z., Ure, K., Ding, P., Nashaat, M., Yuan, L., Ma, J., Hammer, R.E., and Hsieh, J. (2011). The master negative regulator REST/NRSF controls adult neurogenesis by restraining the neurogenic program in quiescent stem cells. *J. Neurosci.* *31*, 9772–9786.
- Ge, W.P., Miyawaki, A., Gage, F.H., Jan, Y.N., and Jan, L.Y. (2012). Local generation of glia is a major astrocyte source in postnatal cortex. *Nature* *484*, 376–380.
- Gohlke, J.M., Armant, O., Parham, F.M., Smith, M.V., Zimmer, C., Castro, D.S., Nguyen, L., Parker, J.S., Gradwohl, G., Portier, C.J., and Guillemot, F. (2008). Characterization of the proneural gene regulatory network during mouse telencephalon development. *BMC Biol.* *6*, 15.
- Guo, Z., Zhang, L., Wu, Z., Chen, Y., Wang, F., and Chen, G. (2014). In vivo direct reprogramming of reactive glial cells into functional neurons after brain injury and in an Alzheimer's disease model. *Cell Stem Cell* *14*, 188–202.
- Heinrich, C., Blum, R., Gascón, S., Masserdotti, G., Tripathi, P., Sánchez, R., Tiedt, S., Schroeder, T., Götz, M., and Berninger, B. (2010). Directing astroglia from the cerebral cortex into subtype specific functional neurons. *PLoS Biol.* *8*, e1000373.
- Heinrich, C., Gascón, S., Masserdotti, G., Lepier, A., Sanchez, R., Simon-Ebert, T., Schroeder, T., Götz, M., and Berninger, B. (2011). Generation of subtype-specific neurons from postnatal astroglia of the mouse cerebral cortex. *Nat. Protoc.* *6*, 214–228.
- Heins, N., Malatesta, P., Cecconi, F., Nakafuku, M., Tucker, K.L., Hack, M.A., Chapouton, P., Barde, Y.A., and Götz, M. (2002). Glial cells generate neurons: the role of the transcription factor Pax6. *Nat. Neurosci.* *5*, 308–315.
- Hirabayashi, Y., and Gotoh, Y. (2010). Epigenetic control of neural precursor cell fate during development. *Nat. Rev. Neurosci.* *11*, 377–388.
- Hubert, O. (2011). Regulation of terminal differentiation programs in the nervous system. *Annu. Rev. Cell Dev. Biol.* *27*, 681–696.
- Huang, W., Sherman, B.T., and Lempicki, R.A. (2009). Systematic and integrative analysis of large gene lists using DAVID bioinformatics resources. *Nat. Protoc.* *4*, 44–57.
- Imayoshi, I., and Kageyama, R. (2014). bHLH factors in self-renewal, multipotency, and fate choice of neural progenitor cells. *Neuron* *82*, 9–23.
- Imura, T., Nakano, I., Kornblum, H.I., and Sofroniew, M.V. (2006). Phenotypic and functional heterogeneity of GFAP-expressing cells in vitro: differential expression of LeX/CD15 by GFAP-expressing multipotent neural stem cells and non-neurogenic astrocytes. *Glia* *53*, 277–293.
- Johnson, R., Teh, C.H., Kunarso, G., Wong, K.Y., Srinivasan, G., Cooper, M.L., Volta, M., Chan, S.S., Lipovich, L., Pollard, S.M., et al. (2008). REST regulates distinct transcriptional networks in embryonic and neural stem cells. *PLoS Biol.* *6*, e256.
- Jørgensen, H.F., Terry, A., Beretta, C., Pereira, C.F., Leleu, M., Chen, Z.F., Kelly, C., Merckenschlager, M., and Fisher, A.G. (2009). REST selectively represses a subset of RE1-containing neuronal genes in mouse embryonic stem cells. *Development* *136*, 715–721.
- Laugesen, A., and Helin, K. (2014). Chromatin repressive complexes in stem cells, development, and cancer. *Cell Stem Cell* *14*, 735–751.
- Laywell, E.D., Rakic, P., Kukekov, V.G., Holland, E.C., and Steindler, D.A. (2000). Identification of a multipotent astrocytic stem cell in the immature and adult mouse brain. *Proc. Natl. Acad. Sci. USA* *97*, 13883–13888.
- Liu, M.L., Zang, T., Zou, Y., Chang, J.C., Gibson, J.R., Huber, K.M., and Zhang, C.L. (2013). Small molecules enable neurogenin 2 to efficiently convert human fibroblasts into cholinergic neurons. *Nat. Commun.* *4*, 2183.
- Livak, K.J., and Schmittgen, T.D. (2001). Analysis of relative gene expression data using real-time quantitative PCR and the 2(-Delta Delta C(T)) Method. *Methods* *25*, 402–408.
- Lu, T., Aron, L., Zullo, J., Pan, Y., Kim, H., Chen, Y., Yang, T.H., Kim, H.M., Drake, D., Liu, X.S., et al. (2014). REST and stress resistance in ageing and Alzheimer's disease. *Nature* *507*, 448–454.
- Martynoga, B., Drechsel, D., and Guillemot, F. (2012). Molecular control of neurogenesis: a view from the mammalian cerebral cortex. *Cold Spring Harb. Perspect. Biol.* *4*, 4.
- Poitras, L., Ghanem, N., Hatch, G., and Ekker, M. (2007). The proneural determinant MASH1 regulates forebrain Dlx1/2 expression through the 112b intergenic enhancer. *Development* *134*, 1755–1765.
- Price, J.D., Park, K.Y., Chen, J., Salinas, R.D., Cho, M.J., Kriegstein, A.R., and Lim, D.A. (2014). The *Ink4a/Arf* locus is a barrier to direct neuronal transdifferentiation. *J. Neurosci.* *34*, 12560–12567.
- Raposo, A.A., Vasconcelos, F.F., Drechsel, D., Marie, C., Johnston, C., Dolle, D., Bithell, A., Gillotin, S., van den Berg, D.L., Ettwiller, L., et al. (2015). *Ascl1* Coordinately Regulates Gene Expression and the Chromatin Landscape during Neurogenesis. *Cell Rep.*, in press. Published online March 4, 2015. <http://dx.doi.org/10.1016/j.celrep.2015.02.025>.
- Schuermans, C., and Guillemot, F. (2002). Molecular mechanisms underlying cell fate specification in the developing telencephalon. *Curr. Opin. Neurobiol.* *12*, 26–34.
- Srinivas, S., Watanabe, T., Lin, C.S., Williams, C.M., Tanabe, Y., Jessell, T.M., and Costantini, F. (2001). Cre reporter strains produced by targeted insertion of EYFP and ECFP into the ROSA26 locus. *BMC Dev. Biol.* *1*, 4.
- Vierbuchen, T., Ostermeier, A., Pang, Z.P., Kokubu, Y., Südhof, T.C., and Wernig, M. (2010). Direct conversion of fibroblasts to functional neurons by defined factors. *Nature* *463*, 1035–1041.
- Voss, A.K., Gamble, R., Collin, C., Shoubridge, C., Corbett, M., Gécz, J., and Thomas, T. (2007). Protein and gene expression analysis of Phf6, the gene mutated in the Börjeson-Forsman-Lehmann Syndrome of intellectual disability and obesity. *Gene Expr. Patterns* *7*, 858–871.
- Wapinski, O.L., Vierbuchen, T., Qu, K., Lee, Q.Y., Chanda, S., Fuentes, D.R., Giresi, P.G., Ng, Y.H., Marro, S., Neff, N.F., et al. (2013). Hierarchical mechanisms for direct reprogramming of fibroblasts to neurons. *Cell* *155*, 621–635.

- Wongtawan, T., Taylor, J.E., Lawson, K.A., Wilmot, I., and Pennings, S. (2011). Histone H4K20me3 and HP1 $\alpha$  are late heterochromatin markers in development, but present in undifferentiated embryonic stem cells. *J. Cell Sci.* *124*, 1878–1890.
- Xue, Y., Ouyang, K., Huang, J., Zhou, Y., Ouyang, H., Li, H., Wang, G., Wu, Q., Wei, C., Bi, Y., et al. (2013). Direct conversion of fibroblasts to neurons by reprogramming PTB-regulated microRNA circuits. *Cell* *152*, 82–96.
- Yoo, A.S., Sun, A.X., Li, L., Shcheglovitov, A., Portmann, T., Li, Y., Lee-Messer, C., Dolmetsch, R.E., Tsien, R.W., and Crabtree, G.R. (2011). MicroRNA-mediated conversion of human fibroblasts to neurons. *Nature* *476*, 228–231.
- Zolles, G., Wagner, E., Lampert, A., and Sutor, B. (2009). Functional expression of nicotinic acetylcholine receptors in rat neocortical layer 5 pyramidal cells. *Cereb. Cortex* *19*, 1079–1091.



**Cell Stem Cell**

**Supplemental Information**

**Transcriptional Mechanisms of Proneural  
Factors and REST in Regulating  
Neuronal Reprogramming of Astrocytes**

**Giacomo Masserdotti, Sébastien Gillotin, Bernd Sutor, Daniela Drechsel, Martin Irmeler,  
Helle F. Jørgensen, Steffen Sass, Fabian J. Theis, Johannes Beckers, Benedikt  
Berninger, François Guillemot, and Magdalena Götz**

Figure S1

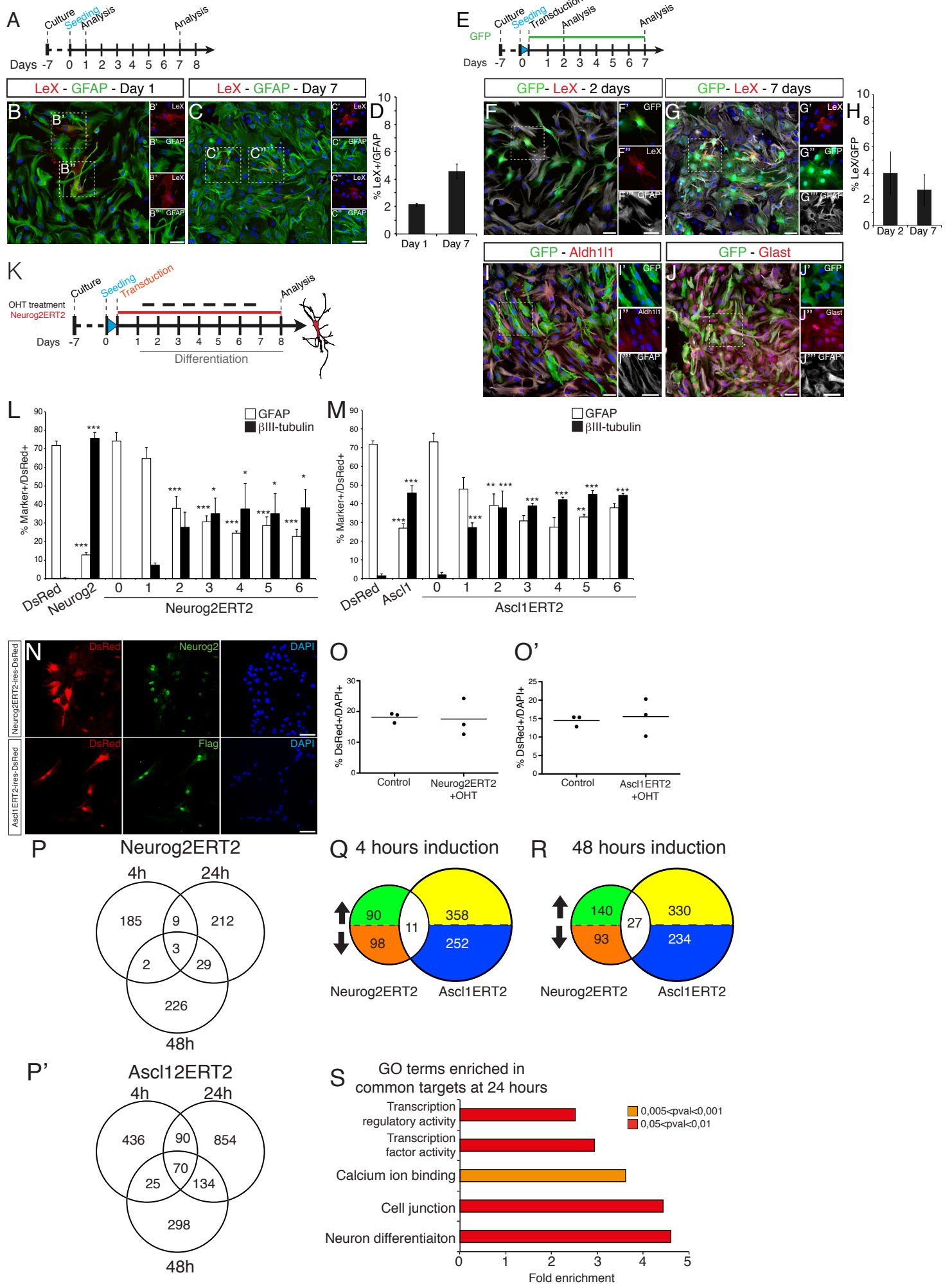


Figure S2

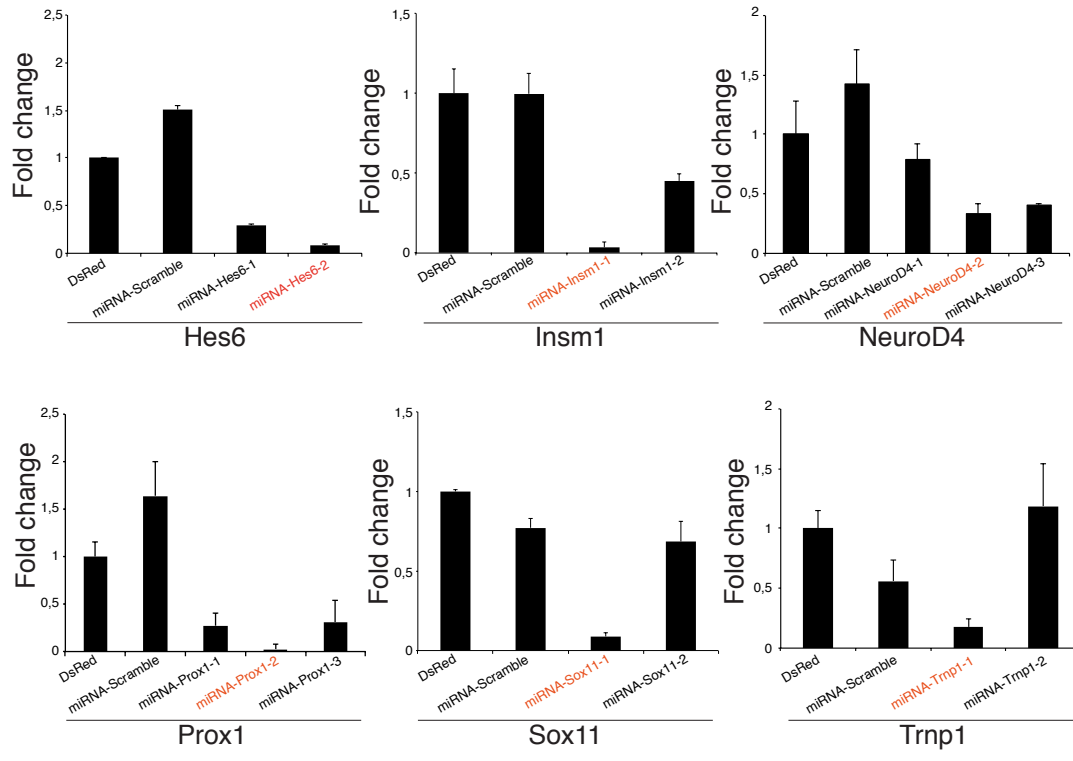


Figure S3

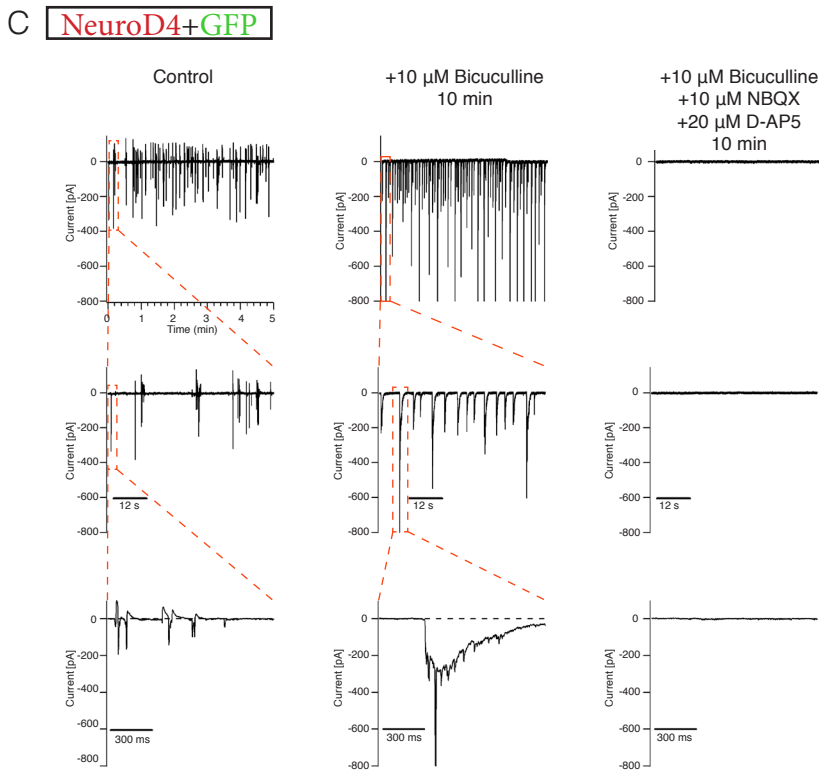
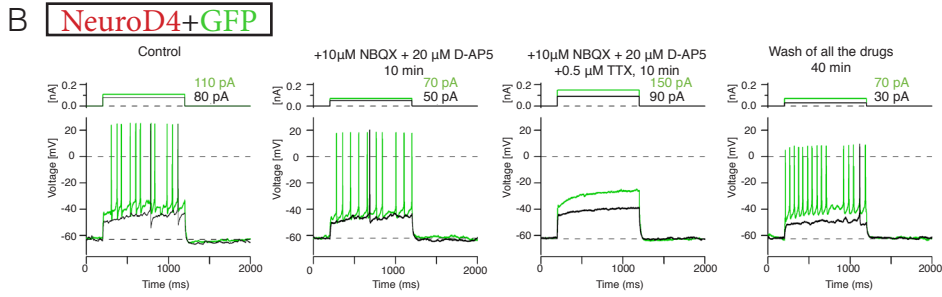
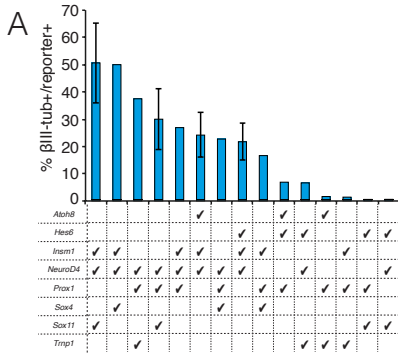




Figure S4

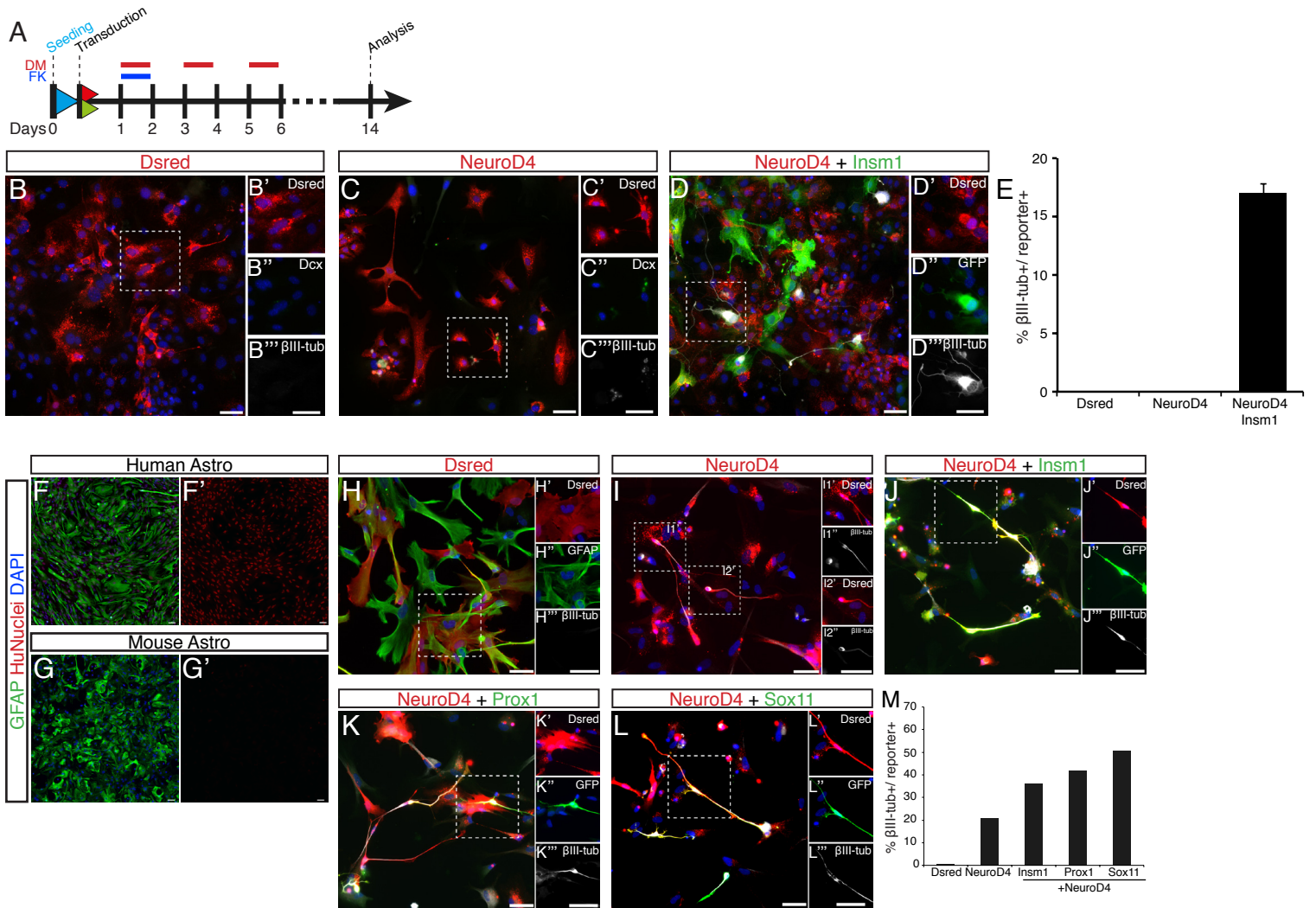


Figure S5

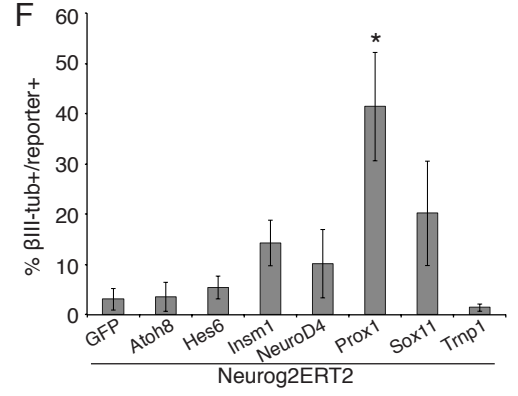
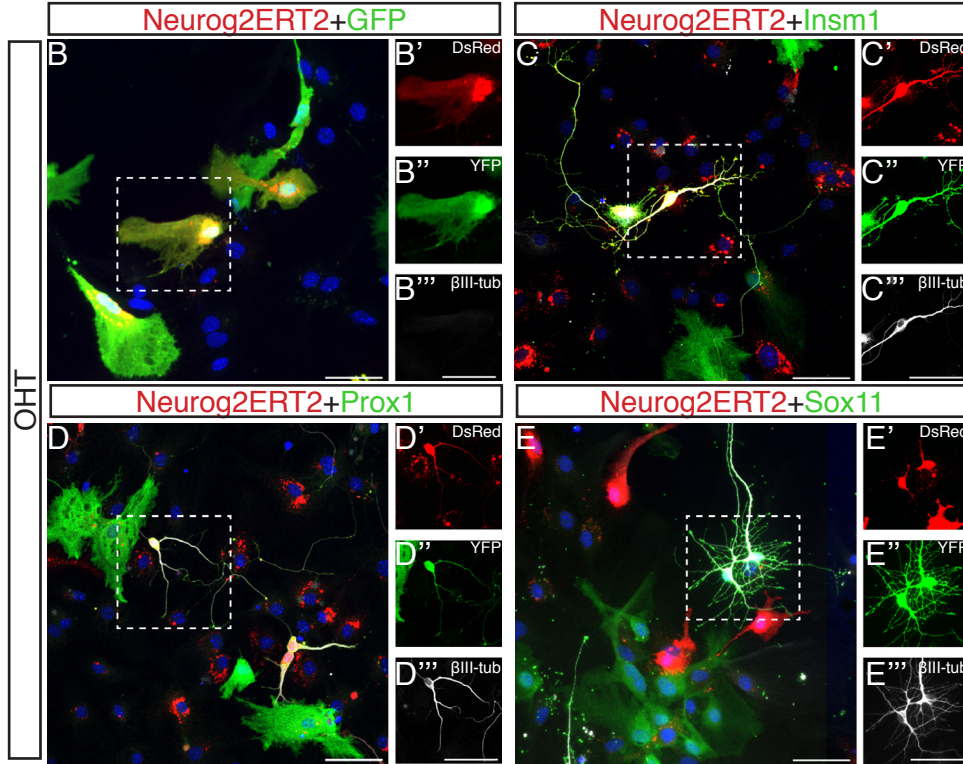
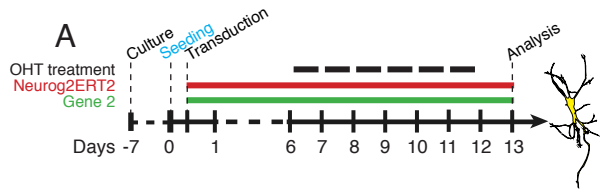


Figure S6

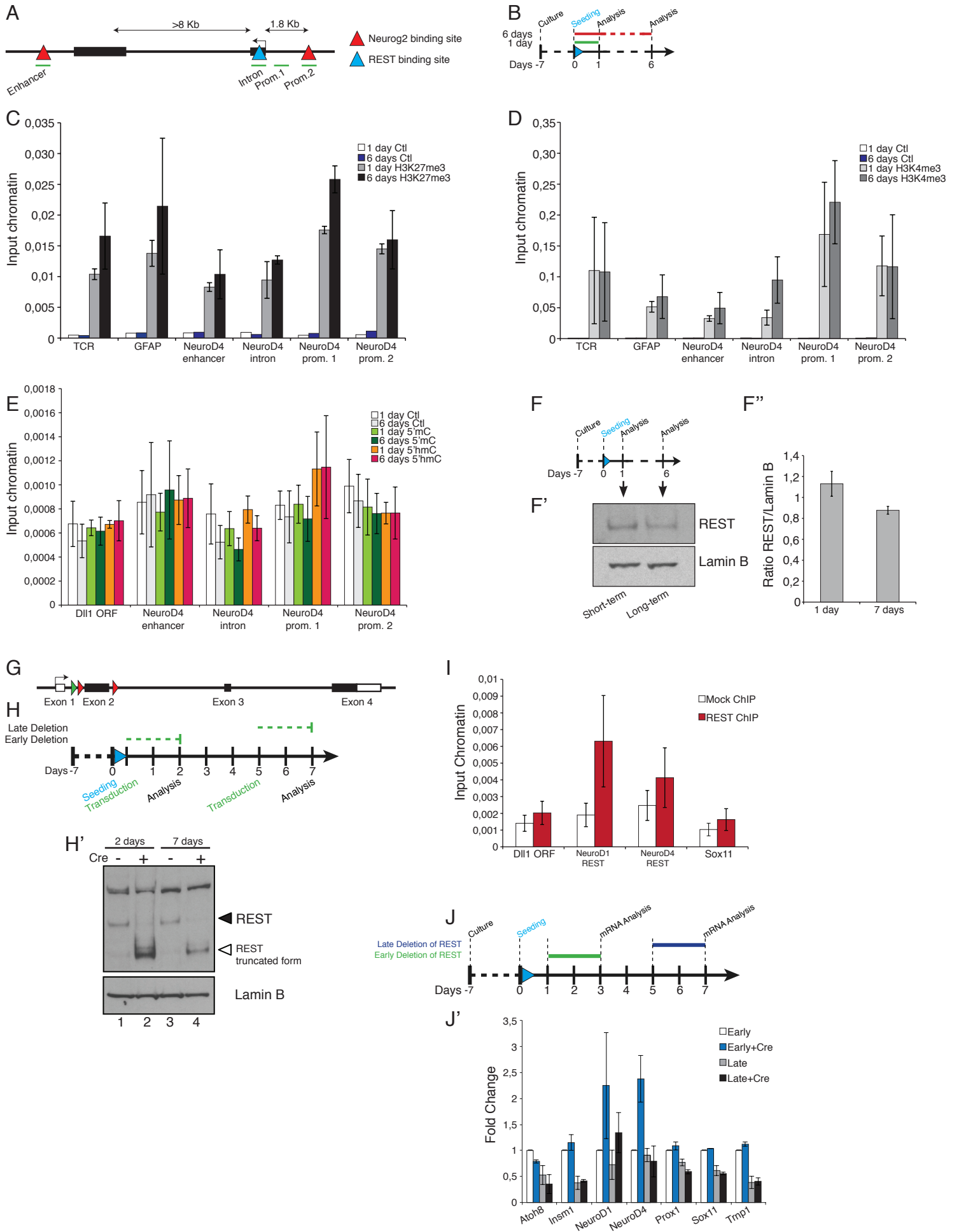
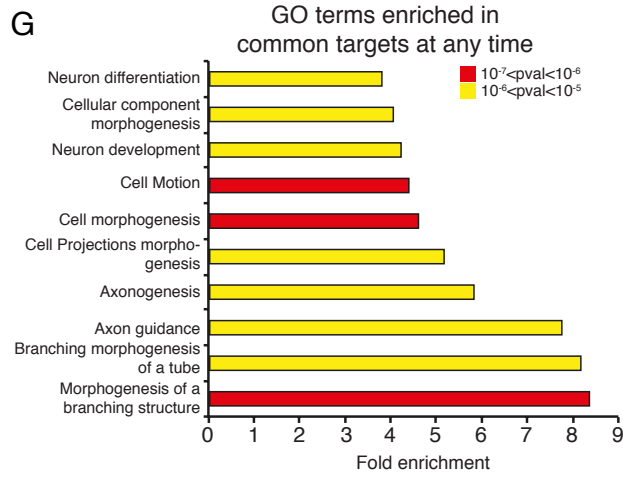
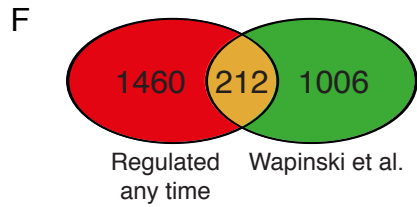
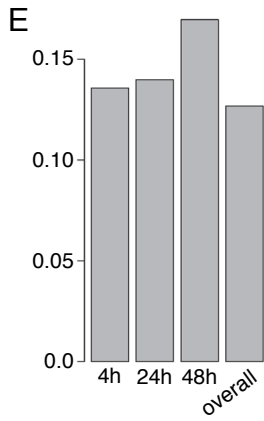
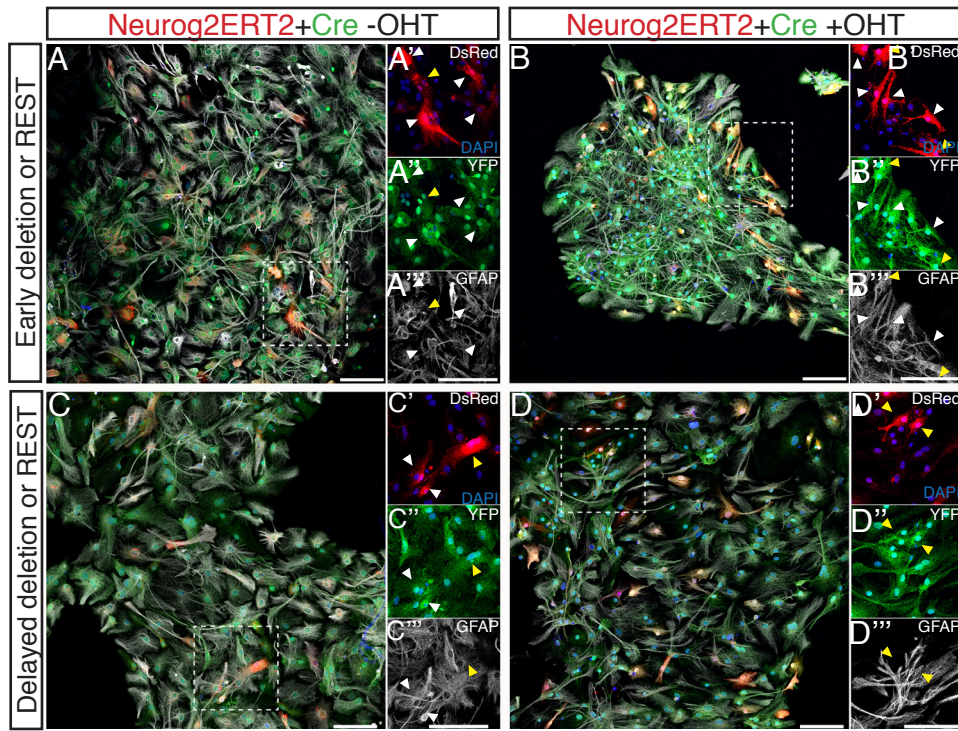


Figure S7





## Supplementary Figure legends

*Figure S1. Related to Figure 1*

*Inducible reprogramming and genome-wide expression analysis*

(A) Schematic drawing of the experimental design for Figure S1B-C.

(B,C) Micrographs of astrocytes 1 day (B) and 7 days (C) after plating immune-positive for LeX (red) and GFAP (green). Scale bar: 100 $\mu$ m.

(D) Histogram showing the proportion of LeX<sup>+</sup> cells/GFAP<sup>+</sup> in astrocytic cultures at day 1 and day 7. (n=3 independent experiment).

(E) Schematic drawing of the experimental design for Fig. S1F-J.

(F-J) Micrograph of GFP-transduced astrocytes at day 2 (F, I, J) and day 7 (G) immunoreactive for LeX (F, G, red), GFAP (F-J, white), Aldh1l1 (I, red) or Glast (J, red).

(H) Histogram showing the proportion of LeX<sup>+</sup>/GFP<sup>+</sup> cells in astrocytic cultures at day 1 and day 7. (n=4 independent experiment).

(K) Schematic drawing of the experimental design.

(L, M) Histograms depicting the proportion of GFAP<sup>+</sup> astrocytes and  $\beta$ III-tubulin<sup>+</sup> neurons after transduction with the constructs indicated and OHT treatment as indicated by the black bar below the histograms. Mean  $\pm$  SEM; n=4 independent experiments; Statistical test ANOVA and Bonferroni's multiple Comparison Test (\*=p<0.05; \*\*\*=p<0.001).

(N) Micrographs depicting astrocytes infected with the constructs indicated on the right side of the panels and immunostained for Neurog2 (green in middle panel of the upper row) or the flag-tag of Ascl1ERT2 (green in middle panel of the lower row) in DsRed-expressing cells at 24 hours after OHT treatment at 2 days post infection. Scale bar: 100 $\mu$ m.

(O-O') Quantification of transduction efficiency in Neurog2ERT2-expressing cells (F), or Ascl1ERT2-transduced cells (F') in absence or presence of OHT for 24 hours.

(P-P') Venn diagrams showing the number of genes significantly regulated in Neurog2ERT2 (P) or Ascl1ERT2 (P') at the time points indicated in the diagrams.

(Q,R) Venn diagram showing the number of genes significantly regulated by Neurog2ERT2 and Ascl1ERT2 at 4 hours (Q) and 48 hours (R) following OHT treatment.

(S) Gene Ontology (GO) terms enriched in the genes regulated by both Neurog2ERT2 and Ascl1ERT2 at 24 hours following OHT treatment.

*Figure S2. Related to Figure 2*

*Validation of microRNA (miRNA)*

Histograms depicting the fold change in expression determined by Real Time qPCR with RNA extracted from cells transfected with the indicated constructs. In red the results obtained with the microRNA selected for further experiments (Figure 2).

*Figure S3. Related to Figure 3 and 4*

*Combinations of downstream targets and characterization of ND4-reprogrammed neurons co-cultured with E14.5 neurons.*

(A) Histogram depicting the proportion of  $\beta$ III-tubulin+ neurons amongst the astrocytes co-transduced with the plasmids indicated on the x-axis in 2-6 independent culture batches depending on the combinations.

(B) Electrophysiological recordings of ND4-reprogrammed neurons at 28-25 DPI. Lack of effects of NBQX and D-AP5 on action potentials (second trace), while addition of TTX blocked the spike induction (third trace) in a reversible manner (fourth trace) (n=3 cells recorded).

(C) Effect of bicuculline addition (middle traces) and NBQX and D-AP5 (right traces) on the reprogrammed neurons. Note that hyperpolarizing events or outward currents recorded under voltage-clamp conditions at -60mV could be inhibited by the GABA<sub>A</sub> receptor antagonist bicuculline. Moreover, the AMPA-receptor antagonist NBQX and the NMDA-receptor antagonist D-AP5 could block the synaptic potentials or currents.

*Figure S4. Related to Figure 4*

*Combinations of downstream targets reprogram murine embryo fibroblasts and human astrocytes*

(A) Schematic drawings of the experiment design for Fig. S4B-E.

(B-D) Example of MEFs transduced with Control (B) NeuroD4 (C) and NeuroD4 and Insm1 (D). Note that only NeuroD4+Insm1 gave rise to  $\beta$ III-tubulin+ (D, D'') cells at 14DPI.

(E) Histogram depicting the proportion of  $\beta$ III-tubulin+ cells among reporter positive cells, (n=3 independent experiment).

(F,G) Human astrocytes are positive for GFAP (G) and the human nuclei marker (F') while mouse astrocytes only for GFAP (G, G'). Scale bar: 100 $\mu$ m.

(H-L) Examples of human astrocytes transduced with retrovirus encoding the indicated genes. Scale bar: 100 $\mu$ m.

(M) Histogram depicting the proportion of  $\beta$ III-tubulin+ cells over the transduced ones. (n=2 independent cultures).

*Figure S5. Related to Figure 5.*

*Expression of downstream targets together with Neurog2ERT2 rescues reprogramming upon Neurog2ERT2 delayed induction.*

(A) Schematic drawing of the co-transduction of Neurog2ERT2 (red) and a second gene (green) followed by delayed activation of Neurog2ERT2.

(B-E) Examples of astrocytes transduced with the Neurog2ERT2 and the indicated factors and analysed 7 days after the first induction. Inserts show that the cells are DsRed+ (B', C', D', E'), GFP+ (B'', C'', D'', E'') and  $\beta$ III-tubulin+ (B''', C''', (D''', E''')). Scale bars= 100 $\mu$ m.

(F) Histogram depicting the proportion of  $\beta$ III-tubulin+ neurons among DsRed/GFP double+ co-transduced cells at 7 days post differentiation. Mean  $\pm$  SEM; n=3 independent experiments; (\*=p<0.05).

*Figure S6. Related to Figure 6.*

*Epigenetic marks at NeuroD4 regulatory regions and analysis of REST expression and function.*

(A) Schematic representation of the mouse *Neurod4* locus. Red and blue triangles represent Neurog2 and REST binding sites respectively and black squares represent exons. Green lines indicate positions of primers used in real time qPCR.

(B) Timeline of sample collection for  $\mu$ ChIP analysis.

(C) H3K27me3  $\mu$ ChIP-PCR on immunoprecipitated material from astroglia collected 1 day or 6 days after plating.

(D) H3K4me3  $\mu$ ChIP-PCR on immunoprecipitated material from astroglia collected 1 day or 6 days after plating.

(E) 5'mC and 5'hmC  $\mu$ ChIP-PCR on immunoprecipitated genomic DNA from astroglia collected 1 day or 6 days after plating.

(F) Timeline of sample collection for Western Blot analysis.

(F'-F'') Western blot analysis of total cell lysate from early and prolonged cultured astroglia. Equal amounts of protein were loaded onto gels and blotted for REST and LaminB (loading control). Note that REST protein levels do not increase during astrocyte maturation in these culture conditions. (F'') Histogram depicting the quantification of the Western blot results as shown in (F') from three independent biological samples with ImageJ, two-tailed unpaired t-test n.s=  $p > 0.05$ .

(G) Schematic representation of the conditional REST mutant allele. The second exon (black square) is flanked by loxP sites (red triangles). The green triangle is the remaining FRT site after neo cassette removal.

(H) Experimental design for early or late REST deletion by Cre in an adenoviral vector added to the cultured astrocytes as indicated.

(H') Western blot of total cell lysate from early and delayed cultures. Cells were transduced with an adenoviral vector serving as a control and lacking Cre (lane 1 and 3) or Cre-encoding adenovirus (lane 2 and 4) for 48 hours. Equal amounts of protein were loaded onto gels and blotted for REST and LaminB (loading control for nuclear proteins). Lower band (empty arrowhead)



is a truncated form of REST lacking exon2, unable to bind DNA (see Figure S6I).

(I) Histogram depicting REST  $\mu$ ChIP-PCR on immunoprecipitated genomic DNA from REST-cKO astrocytes collected 48 hours after infection with Cre-expressing adenovirus. No significant difference was observed between mock ChIP and REST-ChIP. The experiments were performed in parallel to those in Fig. 6B: note that in Fig. 6B the enrichment is 4-5 time higher, indicating an almost complete loss of REST expression.

(J) Timeline of mRNA analysis following Cre-mediated REST deletion.

(J') Histogram depicting the expression of selected genes determined by real-time qPCR upon early or delayed REST deletion. Note that *NeuroD1* and *NeuroD4* are expressed at higher levels upon early REST deletion but not following late REST ablation.

*Figure S7. Related to Figure 7.*

*GFAP expression upon REST deletion.*

(A-D) Examples of GFAP (white) expression in REST<sup>flox</sup> astrocytes transduced with Neurog2ERT2 (red), Cre (green) in the absence (A) or presence of (OHT) according to the scheme in Figure 7 (A,B early deletion; C,D delayed deletion). Scale bar: 100 $\mu$ m.

(E) Histogram depicting the proportion of Ascl1-regulated genes common to a specific time point analysed in the present study and genes regulated in (Wapinski et al., 2013), compared to genes regulated at a specific time point.

(F) Venn diagram showing genes regulated by Ascl1ERT2 in our analysis at any time and Ascl1 in Wapinski et al., 2013 (see Table S7 for gene list).

(G) GO term analysis (Biological Processes) performed on the common genes at any time (212).

## Supplemental Table legends

**Table S1, related to Figure 1.** Overview of regulated genes upon Neurog2ERT2 induction.

**Table S2, related to Figure 1.** Gene Ontology (GO) terms associated with genes regulated by Neurog2ERT2 after 4 hours of OHT treatment. Analysis was performed using DAVID analysis tool. Cut off pValue<0.05.

**Table S3, related to Figure 1.** Overview of regulated genes upon Ascl1ERT2 induction.

**Table S4, related to Figure 1.** GO terms associated with genes regulated by Ascl1ERT2 after 4 hours of OHT treatment. Analysis was performed using DAVID analysis tool. Cut off pValue<0.05.

**Table S5, related to Figure 1.** GO terms associated with genes regulated by both Neurog2ERT2 and Ascl1ERT2 after 24 hours of OHT treatment. Analysis was performed using DAVID analysis tool. Cut off pValue<0.05.

**Table S6, related to Figure 1.** Overview of probesets regulated by Neurog2ERT2 and Ascl1ERT2 after 24 of OHT treatment. Pan-neuronal genes are indicated in red, genes associated with neurons with some regional differences in orange, or genes not directly associated with neuronal expression in black.

**Table S7, related to Figure 7.** Overview of genes commonly regulated by Ascl1ERT2 after OHT at any time and genes regulated by Ascl1 in Wapinski et al. 2013. Genes in red are associated with nervous system expression, in blue genes associated with neuronal expression, and in black genes not directly related to neuronal expression.

**Table S5**

Overview of GO terms associated with genes regulated by both Neurog2ERT2 and Ascl1ERT2 after 24 hours of OHT treatment, related to Figure 1

Category	GO number	Term	PValue	Fold Enrichment	Genes
SP_PIR_KEYWORDS		neurogenesis	4,29E-04	13,77623457	SEMA5A, HES5, SOX11, NEUROD4, SLIT1
SP_PIR_KEYWORDS		differentiation	8,71E-04	6,037584541	SEMA5A, HES5, SOX11, NEUROD4, HES6, CBFA2T3, SLIT1
GOTERM_MF_FAT	GO:0005509	GO:0005509~calcium ion binding	0,004706859	3,615782313	SMOC2, NPTX1, CADM3, TESC, LRP8, SYT7, SLIT1, CALM1
SP_PIR_KEYWORDS		calcium	0,008647342	3,799300806	SMOC2, NPTX1, CADM3, TESC, LRP8, SYT7, CALM1
SP_PIR_KEYWORDS		developmental protein	0,014192435	3,411902812	SEMA5A, HES5, SOX11, NEUROD4, HES6, PROX1, SLIT1
SP_PIR_KEYWORDS		methylation	0,017070488	7,181096028	GNG4, RASD1, RASD2, CALM1
GOTERM_BP_FAT	GO:0030182	GO:0030182~neuron differentiation	0,020559345	4,602045655	SEMA5A, HES5, NEUROD4, SLIT1, TUBB3
GOTERM_CC_FAT	GO:0030054	GO:0030054~cell junction	0,022229501	4,434042553	CADM3, LIMA1, 9030425E11RIK, SYT7, HOMER2
GOTERM_MF_FAT	GO:0030528	GO:0030528~transcription regulator activity	0,030442265	2,518455342	MYCL1, HES5, RCOR2, SOX11, NEUROD4, HES6, CBFA2T3, PROX1
GOTERM_MF_FAT	GO:0003700	GO:0003700~transcription factor activity	0,045757161	2,935493373	MYCL1, RCOR2, SOX11, HES6, CBFA2T3, PROX1
SP_PIR_KEYWORDS		prenylation	0,049635458	8,208735632	GNG4, RASD1, RASD2

## Supplementary Experimental Procedures

### *Cell Culture*

Astrocytes were expanded in uncoated plastic flasks, and, after one week harvested using trypsin/EDTA (Gibco) and plated onto poly-D-lysine (Sigma-Aldrich) coated glass coverslips in 24-well plates (BD Biosciences) at a density of 50,000 cells per well or in uncoated 3 cm dishes (Nunc) at a density of 100,000 cells per dish in fresh and complete astrocyte medium (DMEM/F12, FBS 10%, B27, EGF 10ng/ml and FGF2 10ng/ml, penicillin/streptomycin). At the start of the experiment, cells were either infected with retroviral particles 4-12 hours after plating or transfected with plasmids 24 hours after seeding; one day later, medium was replaced with differentiation medium (DMEM/F12 medium enriched with GlutaMAX (Gibco), penicillin/streptomycin and B27 supplement (Gibco)) to allow neuronal differentiation.

Mouse embryo fibroblasts were grown in complete medium (DMEM, FBS 10%, penicillin/streptomycin). After 3 to 4 passages, cells were harvested using trypsin/EDTA (Gibco) and plated onto poly-D-lysine (Sigma-Aldrich) coated glass coverslips in 24-well plates (BD Biosciences) at a density of 25,000 cells per well in complete medium, and, after 4-12 hours, transduced with retroviruses. 24-36 hours later, complete medium was removed and differentiation medium was added. To improve survival, cells were treated with Forskolin (Sigma) and Dorsomorphin (Sigma) as described (Liu et al., 2013).

Human astrocytes were expanded in Astromedium (ScienCell) and plated onto poly-L-lysine (2 $\mu$ g/ml) at a density of 50,000 cells/well in 24-well plates (BD Biosciences). Cells were transduced with retroviruses 4-12 hours after plating and, one day later, the medium was replaced with differentiation medium. At 8 DPI, cells were fixed and analyzed by immunostaining. Cortical neurons were isolated from E14.5 embryos as previously described (Heins et al., 2002), and 40,000 cells were plated onto reprogrammed cultures.



### *Cloning procedures*

Atoh8 cDNA, kindly provided by Prof. R. Kageyama, was excised from pCLIG-Atoh8 (Inoue et al., 2001), cloned into pENTRY1A (Life Technology) and, then, recombined with the retroviral plasmid pCAG-(Dest)-ires-GFP; Prox1 cDNA, a gift of Dr. P.K. Politis (Kaltezioti et al., 2010), was excised from pEGFP-Prox1, cloned into pENTRY4 and subsequently recombined with the retroviral plasmid pCAG-(Dest)-ires-GFP; Insm1 cDNA, from Prof. W. Huttner (Farkas et al., 2008) was excised from pTOPO-Insm1, cloned into pENTRY4 and subsequently recombined with the retroviral plasmid pCAG-(Dest)-ires-GFP; Hes6, purchased from OpenBiosystems (ThermoScientific), was recombined from pCMVSPORT-Hes6 into pDONR221 (Life Technologies) after removing the 3'UTR, and subsequently recombined with the retroviral plasmid pCAG-(Dest)-ires-GFP; NeuroD4 coding sequence, purchased from OpenBiosystems (ThermoScientific), was excised from pCMVSPORT-NeuroD4, cloned into pENTR1A and recombined with the retroviral plasmid pCAG-(Dest)-ires-Dsred; Sox4 and Sox11 are gift from Prof. D. Chichung Lie (Mu et al., 2012), Trnp1 (Stahl et al., 2013).

### *Micro-Chromatin immunoprecipitation ( $\mu$ ChIP) and qPCR*

Around 100,000 cells per sample were fixed sequentially with di(N-succimidyl) glutarate and 1% formaldehyde in phosphate-buffered saline, then lysed in 100 $\mu$ l of SDS lysis buffer (0.5% SDS, 10mM EDTA, 50mM Tris-HCl pH8.0) supplemented with protease inhibitor cocktail (Roche), sonicated for 10 min, and diluted 5 times in IP buffer (0.2M HEPES pH8.0, 2M NaCl, 0.02M EDTA, 0.1% Na-DOC, 1% Triton X-100, 1mg/ml BSA, protease inhibitor cocktail). Immunoprecipitations (for antibodies and dilutions see Supplementary Experimental procedures) were followed by 5X washing with modified RIPA buffer (50mM HEPES pH7.6, 1mM EDTA, 1% NP-40, 1% Na-DOC, 0.5M LiCl) 5X and with Tris-EDTA buffer (10mM Tris-HCl pH8, 1mM EDTA) 1X and elution with 50  $\mu$ l of IP elution buffer (50mM NaHCO<sub>3</sub>, 1% SDS) twice with vortexing for 15 min which were then combined to a clean tube to reverse cross-linking with 0.45M NaCl at 95°C for 15 min. Samples were treated with

proteinase K and purified using QIAquick MINelute column (Qiagen). Quantities of immunoprecipitated DNA were calculated by comparison with a standard curve generated by serial dilutions of input DNA using a 7500 Real-Time PCR System (Applied Biosystems) and a SYBR green-based kit for quantitative PCR (iQ Supermix, Bio-Rad). The data were plotted as means of at least three independent ChIP assays and two independent amplifications. Antibodies and dilutions used for micro-Chromatin immunoprecipitation: rabbit anti-H3K4me3 (0.25  $\mu$ g per ChIP sample; Millipore, 07-473), mouse anti-H3K27me3 (0.25  $\mu$ g per ChIP sample; Abcam, ab6002), mouse anti-H4K20me3 (0.75  $\mu$ g per ChIP sample; ActiveMotif, clone 6F8-D9), mouse anti-5'mC (0.4  $\mu$ g per ChIP sample; Abcam, ab10805), rabbit anti-5'hmC (0.4  $\mu$ g per ChIP sample; ActiveMotif, 39791), rabbit anti-REST (0.75  $\mu$ g per ChIP sample; Millipore, 07-579) or rabbit anti-HA (0.5  $\mu$ g per ChIP sample; Abcam, ab9110).

Below the list of primers used for ChIP experiments:

Gene Name	Primer forward	Primer Reverse
Atoh8_enh	GAGCCAGCCAAAGTGCTAAC	GGACACAGCCAGATGGTCTT
Cnpy3	CTGGGTAACCACGGCAAC	TCCTCTCATTGGCTATAAAGCAG
Dll1 ORF	GTCTCAGGACCTTCACAGTAG	GAGCAACCTTCTCCGTAGTAG
Insm1_intron	GTGTCCGCTGAGTCCTTCC	AGAACGCAGTGCCCATCTT
Neurod1_prom	GAACCACGTGACCTGCCTAT	GTCCGCGGAGTCTCTAACTG
Neurod1_REST	TAACTGATTGCACCAGCCCTTCT	ACTCGGTGGATGGTTCGTGTTT GA
Neurod4_prom2	AAAAGGAGACCAGACCAGCA	GGGTGGGGTGTAACAGATTG
Neurod4_enh	TACTGTGGGGGTGGGAGTAG	CTAGGGCAAGCTAGGGAAGA
Neurod4_REST	CCCGCGAGTAGTTCTTTCAG	CTACCCTGTGGGCAACATCT
Prox1_prom	CCAGGACGCAGGTCTTTTT	TACTTTTCCGAGCCTTCCTC
Sox11_prom	TTCAAAGAAATCCGCGAGT	ATCTGCACTGGGGTTCAGTC
Trnp1_enh	CCATACCCACAATCCCTCTG	GCCAAAGGACCAGAGTTGTG

#### *Transfection of mouse postnatal astroglia cultures*

For transfection DNA-liposome complexes were prepared in Optimem medium (Invitrogen) using the retroviral plasmids previously described and Lipofectamine 2000 (L2K, Invitrogen). Astrocyte cultures were exposed to DNA-liposome complexes at a concentration of 0.6  $\mu$ g DNA with 0,75 $\mu$ l L2K per 400  $\mu$ l of OptiMEM medium for 4 hours; then the transfection medium was replaced by fresh astrocyte medium and, one day later, the medium was changed with the differentiation medium.

### *Viral particle production*

Viral vectors were produced with a vesicular stomatitis virus pseudotype at titers of  $10^{8-11}$  as determined on HEK cells, and cells were infected about 12 hours after splitting as described above (Heinrich et al., 2011). Cells were allowed to differentiate accordingly to the experiment performed.

### *MicroRNA generation, validation and subcloning*

Gene specific MicroRNAs were designed using the Invitrogen miRNA Designer Center (<https://rnaidesigner.lifetechnologies.com/rnaiexpress/setOption.do?designOption=mirna>) and cloned in pCDNA6.2eGFP according to manufacturer's instructions. To test microRNA knock-down efficiency, HEK cells were transfected using Lipofectamine2000 (Invitrogen) with a vector encoding for the gene of interest and a DsRed-expressing control plasmid, and alternatively with a control plasmid (GFP), a scramble-eGFP-miRNA or gene-specific-eGFP-miRNA. 48 hours later, cells were harvested, RNA was extracted using RNeasy MicroPlus Kit (Qiagen), quantified, retro-transcribed and analyzed by real time quantitative PCR as described previously. Gene expression was evaluated on the basis of cDNA content (human Gapdh expression,  $\Delta\Delta C_t$  method (Livak and Schmittgen, 2001) and normalized to the transfection efficiency (DsRed expression). Each sample was analyzed in triplicate. Primers used are listed below.

### *Immunocytochemistry*

Cells were fixed in 4 % paraformaldehyde (PFA) in phosphate buffered saline (PBS) for 10 min at room temperature (RT), washed in PBS and pretreated in 0.5% Triton X-100 in PBS for 30 min, followed by incubation in 3% BSA and 0.5% Triton X-100 in PBS for 30 min. Primary antibodies were incubated on specimens at room temperature for 2 hours in 2% BSA, 0.5% Triton X-100 in PBS. The following primary antibodies were used: anti-Neurog2 (monoclonal anti-IgG2a, kindly provided by Dr. David Anderson, Howard Hughes Medical

Institute); anti-Flag (polyclonal, rabbit 1: 400, Sigma-Aldrich, F7425); anti-Green Fluorescent Protein (polyclonal GFP, chicken, 1:400, Aves Labs, GFP-1020); anti-Glial Fibrillary Acidic Protein (polyclonal GFAP, rabbit, 1:1000, DakoCytomation, Z0334; mouse monoclonal IgG1, 1:300, Sigma-Aldrich NB G3893); anti-GLAST (ACSA1, Milteny Biotec, 1:300, 130-095-822); Anti-Aldh1l1 (monoclonal IgG1, 1:200, Millipore MAB N495); anti-Red Fluorescent Protein (RFP, polyclonal rabbit, 1:1000, Rockland 600-401-379; rat monoclonal IgG2a 1:300, Chromotek); anti  $\beta$ III-tubulin (mouse IgG2b, 1:500, Sigma, T8660); anti MAP2 (polyclonal rabbit, 1:300, Miltenyi Biotec, AB 5622; mouse monoclonal IgG1, 1:300, Millipore, MAB 378); anti-vGlut1 (polyclonal rabbit, 1:300, Synaptic Systems, 135302); anti-vGAT (polyclonal guine pig, 1:500, Synaptic Systems, 131004); anti-LeX (monoclonal mouse, Santa Cruz, sc-21702), anti-pSMAD1-5 (polyclonal rabbit, 41D10, Cell Signaling), anti-nuclei (monoclonal mouse MAB1281, Chemicon). After washing in PBS, cells were incubated with appropriate species- or subclass-specific secondary antibodies conjugated to Cy<sub>TM</sub>2, Cy<sub>TM</sub>3, Cy<sub>TM</sub>5 (1:500, Jackson ImmunoResearch), Alexa Fluor 488 (1:500, Invitrogen), FITC (fluorescein isothiocyanate, 1:500, Jackson ImmunoResearch), TRITC (tetramethyl rhodamine isothiocyanate, 1:500, Jackson ImmunoResearch) or biotin (1:500, Jackson ImmunoResearch or Vector Laboratories) for 2h in the dark at room temperature, followed by extensive washing in PBS. Following treatment with secondary antibodies conjugated to biotin, cells were subsequently incubated for 2h at room temperature with Alexa Fluor 405 streptavidin (1:500, Invitrogen), or stained with DAPI, then mounted with Aqua Poly/Mount (Polysciences, Warrington, PA).

### *Microarray Analysis*

Total RNA, isolated with the RNeasy Micro Plus Kit, was analyzed with The Agilent 2100 Bioanalyzer and only high quality RNA (RIN>7) was used for microarray analysis. Total RNA (120 ng) was amplified using the one-cycle MessageAmp Premier labeling kit (Ambion). 10  $\mu$ g of amplified aRNA were hybridized on Affymetrix Mouse Genome 430 2.0 arrays containing about



45,000 probe sets. Staining and scanning were done according to the Affymetrix expression protocol Expression console (v.1.2, Affymetrix) was used for quality control and to obtain annotated normalized RMA data (standard settings including quantile normalisation). Statistical analysis of the microarrays was performed by utilizing the statistical programming environment R (C., 2005) implemented in CARMAweb (Rainer et al., 2006). Genewise testing for differential expression was done employing the paired limma *t*-test. *p*-values<0.01 were used to define sets of regulated genes, which were further filtered for fold-changes>1.2x and average expression in one group>10. Heatmaps were generated with CARMAweb.

Below the list of primers used for the Real Time qPCR:

Gene Name	Accession number	Primer forward	Primer reverse	Probe #	Ampl. Length
Atoh8	NM_153778.3	tcagcttccgagtggtg	tagcctgtggcaggctcact	29	91
Atoh8-Cod	NM_153778.3	caaagccctgcagcagac	ggagtagcacggcacctg	73	112
Cnr1	NM_007726.3	gggcaaatctctgtagca	ggctcaacgtgactgagaaa	79	130
Dll3	NM_007866.2	ctgctgatggcctcgta	gctgctctccaggttca	7	85
Dlx2	NM_010054.2	gcctcaccxaaactcaggt	aggcacaaggaggagaagc	1	126
Gapdh (human)	NM_002046	agccacatcgctcagacac	goccaatacagcaaatcc	66	60
Gapdh (mouse)	BC083065	ttcaccaccatggagaagg	cacaccatcacaaacatgg	29	102
Hes6	NM_019479.3	acggatcaacgagagcttca	ttcttagcttggcctgcac	66	72
Insm1	NM_016889.3	ggttctctgctaccaat	tcacccaaaacaaccgta	108	62
Lmo1	NM_057173	ccggcgtgactactctgag	aagctgggatcagcttgc	27	71
NeuroD1	NM_010894.2	cgcagaaggcaaggtgtc	tttgctcatgtttccactcc	1	90
NeuroD4	NM_007501.4	actactcgcgggagctgac	ccatccaggattgtgtttg	22	104
NeuroD4-cod	NM_007501.4	aactggggcctcaatctacc	agtcacaaattgaagattttcctc	80	60
Phf6	NM_027642.1	ggaaataaaagaggcacaagc	gtttcacatcacagccaatg	1	78
Prox1	NM_008937.2	cgacatctaccttattcagga	ttgcctttcaagtattgg	4	68
pvalb	NM_013645	ggcaagattggggtgaag	agcagtcagcgccacttag	83	63
Sfrp1	NM_013834.3	atgtgctccagaagcagacc	gtcagagcagccaacatgc	80	60
Sox11	NM_009234.6	gagctgagcagatgatcg	gaacaccaggtcggagaagt	20	60
Trnp1	NM_001081156.2	agtcagctgggggtccat	atgcagaagtcagtcagacc	110	87
Trnp1-Cod	NM_001081156.2	ctgcaccgagcttcttgg	gcgacccttcttgagac	71	133

### *Microscopy and quantification*

Immunostainings were analyzed with a LSM710 laser-scanning confocal or Axio Observer Z1 epifluorescence microscope (Carl Zeiss). Digital images were captured using the ZEN2009-2011 software (Carl Zeiss). Retroviral vector-transduced cells or transfected cells were quantified from more than 30 randomly chosen 20x fields in at least 3 independent experiments. Branch quantification was performed using the plug-in “Simple Neurite Tracer” (Longair et al., 2011) for the image software in Fiji (Schindelin et al., 2012).

### *Electrophysiology*

For electrophysiological recordings, coverslips with reprogrammed cells were transferred to an organ bath mounted on the stage of an upright microscope (Axioscope FS, Zeiss, Göttingen, Germany). Cells on coverslips were perfused with a bathing solution consisting of (in mM): NaCl 150, KCl 3, CaCl<sub>2</sub> 3, MgCl<sub>2</sub> 2, 4-(2-hydroxyethyl)-1-piperazineethanesulfonic acid (HEPES) 10, and D-glucose 10. The pH of the solution was adjusted to 7.4 (NaOH) and its osmolarity ranged between 309 to 313 mOsmol. The perfusion rate with bathing solution (see Main Materials and Methods) was set to 1.4 ml / min and recordings were performed at room temperature (23 – 24°C). In order to visualize the cultured cells, the microscope was equipped with differential interference contrast (DIC) optics and with epifluorescence optics for green and red fluorescence (filter sets: Zeiss BP450-490, LP520, Zeiss BP546/12, IP590). Images were taken and displayed using a software-operated CCD microscope camera (ORCA R, Hamamatsu, Herrsching, Germany).

The recorded signals were amplified (x10 or x20), filtered at 10 or 20 kHz (current clamp) and 3 kHz (voltage clamp), digitized at a sampling rate of 10 or 20 kHz and stored on a computer for off-line analysis. Data acquisition and generation of command pulses was done by means of a CED 1401 Power 3 system in conjunction with Signal6 data acquisition software (Cambridge electronic design, Cambridge, England). Data analysis was performed using IGOR Pro 6 (WaveMetrics, Lake Oswego, USA) together with the NeuroMatic IGOR plugin ([www.neuromatic.thinkrandom.com](http://www.neuromatic.thinkrandom.com)). The action potential discharge pattern of the cells was investigated by injections of depolarizing current pulses (1 – 2 s), the amplitudes of which were raised in steps (5 or 10 pA) from 0 – 200 pA at a frequency of 0.1 Hz.

The electrodes for whole cell patch-clamp recordings were fabricated from borosilicate glass capillaries (OD: 1.5 mm, ID: 0.86 mm, Hugo Sachs Elektronik-Harvard Apparatus, March-Hugstetten, Germany) and filled with a solution composed of (in mM): potassium gluconate 135, KCl 4, NaCl 2, ethylene glycol-bis(2-aminoethylether)-N,N,N',N'-tetraacetic acid (EGTA) 0.2, HEPES (potassium salt) 10, adenosine-triphosphate (magnesium salt,

ATP[Mg]) 4, sodium guanosine-triphosphate (NaGTP) 0.5, and phosphocreatine 10 (pH: 7.25 – 7.30, osmolarity: 288 – 291 mOsmol). The electrodes (resistance: 5 – 6 MW) were connected to the headstage of a npi ELC-03XS amplifier (npi, Tamm, Germany). The series resistance determined after establishment of the whole cell recording mode (9 – 17 MW) was compensated by 70 – 85%. Microscope images were corrected for contrast and brightness with Photoshop CS3 (Adobe Software Systems, Ireland).

By using the motorized microscope stage, each coverslip was scanned systematically and reprogrammed cells were identified by their simultaneous green and red fluorescence. Following membrane rupture, the cells were voltage-clamped to a holding potential of -60 mV and kept under this condition until stabilization of the holding current was achieved (3 – 5 min). Then the amplifier was switched to the current-clamp mode and the resting membrane potential was registered. Determination of the input resistance  $R_N$  was performed either by measurement of the amplitude of a voltage deviation induced by a small hyperpolarizing current pulse (1 s, 5 – 10 pA) or by determining the slope of the current-voltage-curve (IV-curve). The somatic membrane time constant  $\tau$  was derived by fitting a dual exponential function to the voltage relaxation following cessation of a small hyperpolarizing current pulse and the total membrane capacity  $C_N$  was estimated using a method described by (Zemankovics et al., 2010). The ability of the cells to generate action potentials was tested by injecting depolarizing current pulses (50 ms) with increasing current strengths (DI: 5 or 10 pA) or by depolarizing current ramps (50 ms) from 0 – 100 pA. The amplitudes of the action potentials (spikes) were measured as the difference between the resting membrane potential and the spike maximum, the spike duration was determined at half-maximum amplitude and the spike threshold was derived from a phase-plane plot (Bean, 2007). The action potential discharge pattern of the cells was investigated by injections of depolarizing current pulses (1 – 2 s), the amplitudes of which were raised in steps (5 or 10 pA) from 0 – 200 pA at a frequency of 0.1 Hz.

All chemicals and drugs were obtained from Sigma-Aldrich (Munich,

Germany) and Biotrend (Cologne, Germany), respectively. The GABA<sub>A</sub>-receptor antagonist bicuculline (methiodide, 10 $\mu$ M), the AMPA receptor antagonist 2,3-dihydroxy-6-nitro-7-sulfamoyl-benzo[f]quinoxaline-2,3-dione (NBQX, 5-10 $\mu$ M), the NMDA receptor antagonist D-2-amino-5-phosphonopentanoate (D-AP5), and the sodium channel blocker tetrodotoxin (TTX) were added to the bathing solution. Data are given as mean and standard deviation (SD). Statistical comparison of 2 samples was performed by using a two-tailed unpaired t-test. Comparisons of 3 or more samples were done by means of a one-way analysis of variance (ANOVA with Bonferroni post-tests).

### *Statistics*

Statistical analyses were performed with GraphPrism 4 software by using 1-way-ANOVA Bonferroni post-test or two-tailed unpaired t-test as indicated in the figures.

## References

- Bean, B.P. (2007). The action potential in mammalian central neurons. *Nature reviews Neuroscience* 8, 451-465.
- C., T.R.D. (2005). R: A Language and environment for statistical computing.
- Farkas, L.M., Haffner, C., Giger, T., Khaitovich, P., Nowick, K., Birchmeier, C., Paabo, S., and Huttner, W.B. (2008). Insulinoma-associated 1 has a panneurogenic role and promotes the generation and expansion of basal progenitors in the developing mouse neocortex. *Neuron* 60, 40-55.
- Heinrich, C., Gascon, S., Masserdotti, G., Lepier, A., Sanchez, R., Simon-Ebert, T., Schroeder, T., Gotz, M., and Berninger, B. (2011). Generation of subtype-specific neurons from postnatal astroglia of the mouse cerebral cortex. *Nature protocols* 6, 214-228.
- Heins, N., Malatesta, P., Cecconi, F., Nakafuku, M., Tucker, K.L., Hack, M.A., Chapouton, P., Barde, Y.A., and Gotz, M. (2002). Glial cells generate neurons: the role of the transcription factor Pax6. *Nature neuroscience* 5, 308-315.
- Inoue, C., Bae, S.K., Takatsuka, K., Inoue, T., Bessho, Y., and Kageyama, R. (2001). Math6, a bHLH gene expressed in the developing nervous system, regulates neuronal versus glial differentiation. *Genes to cells : devoted to molecular & cellular mechanisms* 6, 977-986.
- Kaltezioti, V., Kouroupi, G., Oikonomaki, M., Mantouvalou, E., Stergiopoulos, A., Charonis, A., Rohrer, H., Matsas, R., and Politis, P.K. (2010). Prox1 regulates the notch1-mediated inhibition of neurogenesis. *PLoS biology* 8, e1000565.
- Liu, M.L., Zang, T., Zou, Y., Chang, J.C., Gibson, J.R., Huber, K.M., and Zhang, C.L. (2013). Small molecules enable neurogenin 2 to efficiently convert human fibroblasts into cholinergic neurons. *Nature communications* 4, 2183.
- Livak, K.J., and Schmittgen, T.D. (2001). Analysis of relative gene expression data using real-time quantitative PCR and the 2(-Delta Delta C(T)) Method. *Methods* 25, 402-408.
- Longair, M.H., Baker, D.A., and Armstrong, J.D. (2011). Simple Neurite Tracer: open source software for reconstruction, visualization and analysis of neuronal processes. *Bioinformatics* 27, 2453-2454.
- Mu, L., Berti, L., Masserdotti, G., Covic, M., Michaelidis, T.M., Doberauer, K., Merz, K., Rehfeld, F., Haslinger, A., Wegner, M., *et al.* (2012). SoxC transcription factors are required for neuronal differentiation in adult hippocampal neurogenesis. *The Journal of neuroscience : the official journal of the Society for Neuroscience* 32, 3067-3080.
- Rainer, J., Sanchez-Cabo, F., Stocker, G., Sturn, A., and Trajanoski, Z. (2006). CARMAweb: comprehensive R- and bioconductor-based web service for microarray data analysis. *Nucleic acids research* 34, W498-503.
- Schindelin, J., Arganda-Carreras, I., Frise, E., Kaynig, V., Longair, M., Pietzsch, T., Preibisch, S., Rueden, C., Saalfeld, S., Schmid, B., *et al.* (2012). Fiji: an open-source platform for biological-image analysis. *Nature methods* 9, 676-682.
- Stahl, R., Walcher, T., De Juan Romero, C., Pilz, G.A., Cappello, S., Irmeler, M., Sanz-Aquela, J.M., Beckers, J., Blum, R., Borrell, V., *et al.* (2013). Trnp1 regulates expansion and folding of the mammalian cerebral cortex by control of radial glial fate. *Cell* 153, 535-549.



Wapinski, O.L., Vierbuchen, T., Qu, K., Lee, Q.Y., Chanda, S., Fuentes, D.R., Giresi, P.G., Ng, Y.H., Marro, S., Neff, N.F., *et al.* (2013). Hierarchical mechanisms for direct reprogramming of fibroblasts to neurons. *Cell* 155, 621-635.

Zemankovics, R., Kali, S., Paulsen, O., Freund, T.F., and Hajos, N. (2010). Differences in subthreshold resonance of hippocampal pyramidal cells and interneurons: the role of h-current and passive membrane characteristics. *The Journal of physiology* 588, 2109-2132.